
Tensorial Mixture Models

Or Sharir

Department of Computer Science
The Hebrew University of Jerusalem
Israel
or.sharir@cs.huji.ac.il

Ronen Tamari

Department of Computer Science
The Hebrew University of Jerusalem
Israel
ronent@cs.huji.ac.il

Nadav Cohen

Department of Computer Science
The Hebrew University of Jerusalem
Israel
cohennadav@cs.huji.ac.il

Amnon Shashua

Department of Computer Science
The Hebrew University of Jerusalem
Israel
shashua@cs.huji.ac.il

Abstract

Casting neural networks in generative frameworks is a highly sought-after endeavor these days. Contemporary methods, such as Generative Adversarial Networks, capture some of the generative capabilities, but not all. In particular, they lack the ability of tractable marginalization, and thus are not suitable for many tasks. Other methods, based on arithmetic circuits and sum-product networks, do allow tractable marginalization, but their performance is challenged by the need to learn the structure of a circuit. Building on the tractability of arithmetic circuits, we leverage concepts from tensor analysis, and derive a family of generative models we call Tensorial Mixture Models (TMMs). TMMs assume a simple convolutional network structure, and in addition, lend themselves to theoretical analyses that allow comprehensive understanding of the relation between their structure and their expressive properties. We thus obtain a generative model that is tractable on one hand, and on the other hand, allows effective representation of rich distributions in an easily controlled manner. These two capabilities are brought together in the task of classification under missing data, where TMMs deliver state of the art accuracies with seamless implementation and design.

1 Introduction

There have been many attempts in recent years to marry generative models with neural networks, including successful methods, such as Generative Adversarial Networks [19], Variational Auto-Encoders [24], NADE [38], and PixelRNN [39]. Though each of the above methods has demonstrated its usefulness on some tasks, it is yet unclear if their advantage strictly lies in their generative nature or some other attribute. More broadly, we ask if combining generative models with neural networks could lead to methods who have a clear advantage over purely discriminative models.

On the most fundamental level, if X stands for an instance and Y for its class, generative models learn $\mathbb{P}(X, Y)$, from which we can also infer $\mathbb{P}(Y|X)$, while discriminative models learn only $\mathbb{P}(Y|X)$. It might not be immediately apparent if this sole difference leads to any advantage. In Ng and Jordan [31], this question was studied with respect to the sample complexity, proving that under *some cases* it can be significantly lesser in favor of the generative classifier. We wish to highlight a more clear cut case, by examining the problem of classification under missing data – where the value of some of the entries of X are unknown at prediction time. Under these settings, discriminative classifiers typically rely on some form of data imputation, i.e. filling missing values by some auxiliary method prior to prediction. Generative classifiers, on the other hand, are naturally suited

to handle missing values through marginalization – effectively assessing every possible completion of the missing values. Moreover, under mild assumptions, this method is optimal *regardless of the process by which values become missing* (see sec. 3).

It is evident that such application of generative models assumes we can efficiently and exactly compute $\mathbb{P}(X, Y)$, a process known as *tractable inference*. Moreover, it assumes we may efficiently marginalize over any subset of X , a procedure we refer to as *tractable marginalization*. Not all generative models have both of these properties, and specifically not the ones mentioned in the beginning of this section. Known models that do possess these properties, e.g. Latent Tree Model [30], have other limitations. A detailed discussion can be found in sec. 4, but in broad terms, all known generative models possess one of the following shortcomings: (i) they are insufficiently expressive to model high-dimensional data (images, audio, etc.), (ii) they require explicitly designing all the dependencies of the data, or (iii) they do not have tractable marginalization. Models based on neural networks typically solve (i) and (ii), but are incapable of (iii), while more classical methods, e.g. mixture models, solve (iii) but suffer from (i) and (ii).

There is a long history of specifying tractable generative models through arithmetic circuits and sum-product networks [12, 34] – computational graphs comprised solely of product and weighted sum nodes. To address the shortcomings above, we take a similar approach, but go one step further and leverage tensor analysis to distill it to a specific family of models we call Tensorial Mixture Models. A Tensorial Mixture Model assumes a convolutional network structure, but as opposed to previous methods tying generative models with neural networks, lends itself to theoretical analyses that allow a thorough understanding of the relation between its structure and its expressive properties. We thus obtain a generative model that is tractable on one hand, and on the other hand, allows effective representation of rich distributions in an easily controlled manner.

2 Tensorial Mixture Models

One of the simplest types of tractable generative models are mixture models, where the probability distribution is defined the convex combination of M mixing components (e.g. Normal distributions): $\mathbb{P}(\mathbf{x}) = \sum_{d=1}^M \mathbb{P}(d)\mathbb{P}(\mathbf{x}|d; \theta_d)$. Mixture models are very easy to learn, and many of them are able to approximate any probability distribution, given sufficient number of components, rendering them suitable for a variety of tasks. The disadvantage of classic mixture models is that they do not scale well to high dimensional data (“curse of dimensionality”). To address this challenge, we extend mixture models, leveraging the fact many high dimensional domains (e.g. images) are typically comprised of small, simple local structures. We represent a high dimensional instance as $X = (\mathbf{x}_1, \dots, \mathbf{x}_N)$ – an N -length sequence of s -dimensional vectors $\mathbf{x}_1, \dots, \mathbf{x}_N \in \mathbb{R}^s$ (called *local structures*). X is typically thought of as an image, where each local structure \mathbf{x}_i corresponds to a local patch from that image, where no two patches are overlapping. We assume that the distribution of individual local structures can be efficiently modeled by some mixture model of few components, which for natural image patches, was shown to be the case [42]. Formally, for all $i \in [N]$ there exists $d_i \in [M]$ such that $\mathbf{x}_i \sim P(\mathbf{x}|d_i; \theta_{d_i})$, where d_i is a hidden variable specifying the matching component for the i -th local structure. The probability density of sampling X is thus described by:

$$P(X) = \sum_{d_1, \dots, d_N=1}^M P(d_1, \dots, d_N) \prod_{i=1}^N P(\mathbf{x}_i|d_i; \theta_{d_i}) \quad (1)$$

where $P(d_1, \dots, d_N)$ represents the prior probability of assigning components d_1, \dots, d_N to their respective local structures $\mathbf{x}_1, \dots, \mathbf{x}_N$. As with classical mixture models, any probability density function $\mathbb{P}(X)$ could be approximated arbitrarily well by eq. 1, as $M \rightarrow \infty$ (see app. A).

At first glance, eq. 1 seems to be impractical, having an exponential number of terms. In the literature, this equation is known as the “Network Polynomial” [12], and the traditional method to overcome its intractability is to express $P(d_1, \dots, d_N)$ by an arithmetic circuit, or sum-product networks, following certain constraints (decomposable and complete). We augment this method by viewing $P(d_1, \dots, d_N)$ from an algebraic perspective, treating it as a tensor of order N and dimension M in each mode, i.e., as a multi-dimensional array, $\mathcal{A}_{d_1, \dots, d_N}$ specified by N indices d_1, \dots, d_N , each ranging in $[M]$, where $[M] \equiv \{1, \dots, M\}$. We refer to $\mathcal{A}_{d_1, \dots, d_N} \equiv P(d_1, \dots, d_N)$ as the *prior tensor*. Under this perspective, eq. 1 can be thought of as a mixture model with tensorial mixing weights, thus we call the arising models *Tensorial Mixture Models*, or TMMs for short.

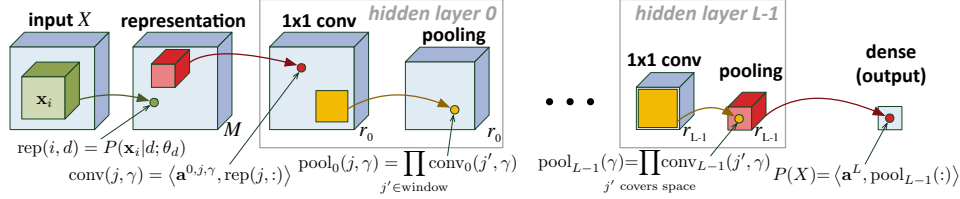


Figure 1: A generative variant of Convolutional Arithmetic Circuits.

2.1 Tensor Factorization, Tractability, and Convolutional Arithmetic Circuits

Not only is it intractable to compute eq. 1, but it is also impossible to even store the prior tensor. We argue that addressing the latter is intrinsically tied to addressing the former. For example, if we impose a sparsity constraint on the prior tensor, then we only need to compute the few non-zero terms of eq. 1. TMMs with sparsity constraints can represent common generative models, e.g. GMMs (see app. B). However, they do not take full advantage of the prior tensor. Instead, we consider constraining TMMs with prior tensors that adhere to non-negative low-rank factorizations.

We begin by examining the simplest case, where the prior tensor \mathcal{A} takes a *rank-1* form, i.e. there exist vectors $\mathbf{v}^{(1)}, \dots, \mathbf{v}^{(N)} \in \mathbb{R}^M$ such that $\mathcal{A}_{d_1, \dots, d_N} = \prod_{i=1}^N v_{d_i}^{(i)}$, or in tensor product notation, $\mathcal{A} = \mathbf{v}^{(1)} \otimes \dots \otimes \mathbf{v}^{(N)}$. If we interpret¹ $v_d^{(i)} = P(d_i=d)$ as a probability over d_i , and so $P(d_1, \dots, d_N) = \prod_i P(d_i)$, then it reveals that imposing a rank-1 constraint is actually equivalent to assuming the hidden variables d_1, \dots, d_N are statistically independent. Applying it to eq. 1 results in the tractable form $P(X) = \prod_{i=1}^N \sum_{d=1}^M P(d_i=d) P(\mathbf{x}_i | d_i, \theta_{d_i})$, or in other words, a product of mixture models. Despite the familiar setting, this strict assumption severely limits expressivity.

In a broader setting, we look at general factorization schemes that given sufficient resources could represent any tensor. Namely, the CANDECOMP/PARAFAC (CP) and the Hierarchical Tucker (HT) factorizations. The CP factorization is simply a sum of rank-1 tensors, extending the previous case, and HT factorization can be seen as a recursive application of CP (see def. in app. C). Since both factorization schemes are solely based on product and weighted sum operations, they could be realized through arithmetic circuits. As shown by Cohen et al. [9], this gives rise to a specific class of convolutional networks named Convolutional Arithmetic Circuits (ConvACs), which consist of 1×1 -convolutions, non-overlapping product pooling layers, and linear activations. More specifically, the CP factorization corresponds to shallow ConvACs, HT corresponds to deep ConvACs, and the number of channels in each layer corresponds to the respective concept of “rank” in each factorization scheme. In general, when a tensor factorization is applied to eq. 1, inference is equivalent to first computing the likelihoods of all mixing components $\{P(\mathbf{x}_i | d_i; \theta_{d_i})\}_{d_i=1, i=1}^{M, N}$, in what we call the *representation* layer, followed by a ConvAC. A complete network is illustrated in fig. 1.

When restricting the prior tensor of eq. 1 to a factorization, we must ensure it represents actual probabilities, i.e. it is non-negative and its entries sum to one. This can be addressed through a restriction to non-negative factorizations, which translates to limiting the parameters of each convolutional kernel to the simplex. There is a vast literature on the relations between non-negative factorizations and generative models [21, 30]. As opposed to most of these works, we apply factorizations merely to derive our model and analyze its expressivity – not for learning its parameters (see sec. 2.3).

From a generative perspective, the restriction of convolutional kernels to the simplex results in a latent tree graphical model, as illustrated in fig. 2. Each *hidden layer* in the ConvAC network – a pair of convolution and pooling operations, corresponds to a transition between two levels in the tree. More specifically, each level is comprised of multiple latent variables, one for each spatial position in the input to a hidden layer in the network. Each latent variable in the input to the l -th layer takes values in $[r_{l-1}]$ – the number of channels in the layer that precedes it.

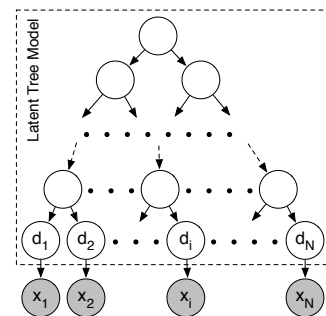


Figure 2: Graphical model description of HT-TMM

¹ \mathcal{A} represents a probability, and w.l.o.g. we can assume all entries of $\mathbf{v}^{(i)}$ are non-negative and $\sum_{d=1}^M v_d^{(i)} = 1$

Pooling operations in the network correspond to the parent-child relationships in the tree – a set of latent variables are siblings with a shared parent in the tree, if they are positioned in the same pooling window in the network. The weights of convolution operations correspond to the transition matrix between a parent and each of its children, i.e. if H_p is the parent latent variable, taking values in $[r_t]$, and H_{child} is one of its child variables, taking values in $[r_{t-1}]$, then $P(H_{child}=i|H_p=c)=w_i^{(c)}$, where $w^{(c)}$ is the 1×1 convolutional kernel for the c -th output channel. With the above graphical representation in place, we can easily draw samples from our model.

To conclude this subsection, by leveraging an algebraic perspective of the network polynomial (eq. 1), we show that tractability is related to the tensor properties of the priors, and in particular, that low rank factorizations are equivalent to inference via ConvACs. The application of arithmetic circuits to achieve tractability is by itself not a novelty. However, the particular convolutional arithmetic circuits we propose lead to a comprehensive understanding of representational abilities, and as a result, to a straightforward architectural design of TMMs.

2.2 Controlling the Expressivity and Inductive Bias of TMMs

As discussed in sec. 1, it is not enough for a generative model to be tractable – it must also be sufficiently expressive, and moreover, we must also be able to understand how its structure affects its expressivity. In this section we explain how our algebraic perspective enables us to achieve this.

To begin with, since we derived our model by factorizing the prior tensor, it immediately follows that given sufficient number of channels in the ConvAC, i.e. given sufficient ranks in the tensor factorization, any distribution could be approximated arbitrarily well (assuming M is allowed to grow). In short, this amounts to saying that TMMs are universal. Though many other generative models are known to be universal, it is typically not clear how one may assess what a given structure of finite size can and cannot express. In contrast, the expressivity of ConvACs has been thoroughly studied in a series of works [9, 8, 11, 27], each of which examined a different attribute of its structure. In Cohen et al. [9] it was proven that ConvACs exhibit the Depth Efficiency property, i.e. deep networks are exponentially more expressive than shallow ones. In Cohen and Shashua [8] it was shown that deep networks can efficiently model some input correlations but not all, and that by designing appropriate pooling schemes, different preferences may be encoded, i.e. the inductive bias may be controlled. In Cohen et al. [11] this result was extended to more complex connectivity patterns, involving mixtures of pooling schemes. Finally, in Levine et al. [27], an exact relation between the number of channels and the correlations supported by a network has been found, enabling tight control over expressivity and inductive bias. All of these results are brought forth by the relations of ConvACs to tensor factorizations. They allow TMMs to be analyzed and designed in much more principled ways than alternative high-dimensional generative models.²

2.3 Classification and Learning

TMMs realized through ConvACs, sharing many of the same traits as ConvNets, are especially suitable to serve as classifiers. We begin by introducing a class variable Y , and model the conditional likelihood $\mathbb{P}(X|Y=y)$ for each $y \in [K]$. Though it is possible to have separate generative models for each class, it is much more efficient to leverage the relation to ConvNets and use a shared ConvAC instead, which is equivalent to a joint-factorization of the prior tensors for all classes. This results in a single network, where instead of a single scalar output representing $\mathbb{P}(X)$, multiple outputs are driven by the network, representing $\mathbb{P}(X|Y=y)$ for each class y . Predicting the class of a given instance is carried through Maximum A-Posteriori, i.e. by returning the most likely class. In the common setting of uniform class priors, i.e. $\mathbb{P}(Y=y) \equiv \frac{1}{K}$, this corresponds to classification by maximal network output, as customary with ConvNets. We note that in practice, naïve implementation of ConvACs is not numerically stable³, and this is treated by performing all computations in log-space, which transforms ConvACs into *SimNets* – a recently introduced deep learning architecture [7, 10].

Suppose now that we are given a training set $S = \{(X^{(i)} \in (\mathbb{R}^s)^N, Y^{(i)} \in [K])\}_{i=1}^{|S|}$ of instances and labels, and would like to fit the parameters Θ of our model according to the Maximum Likelihood

² As a demonstration of the fact that ConvAC analyses are not affected by the non-negativity and normalization restrictions of our generative variant, we prove in app. D that the Depth Efficiency property still holds.

³ Since high degree polynomials (as computed by ACs) are susceptible to numerical underflow or overflow.

principle, or equivalently, by minimizing the Negative Log-Likelihood (NLL) loss function: $\mathcal{L}(\Theta) = \mathbb{E}[-\log \mathbb{P}_\Theta(X, Y)]$. The latter can be factorized into two separate loss terms:

$$\mathcal{L}(\Theta) = \mathbb{E}[-\log \mathbb{P}_\Theta(Y|X)] + \mathbb{E}[-\log \mathbb{P}_\Theta(X)]$$

where $\mathbb{E}[-\log \mathbb{P}_\Theta(Y|X)]$, which we refer to as the *discriminative loss*, is commonly known as the cross-entropy loss, and $\mathbb{E}[-\log \mathbb{P}_\Theta(X)]$, which corresponds to maximizing the prior likelihood $\mathbb{P}(X)$, has no analogy in standard discriminative classification. It is this term that captures the generative nature of the model, and we accordingly refer to it as the *generative loss*. Now, let $N_\Theta(X^{(i)}; y) := \log \mathbb{P}_\Theta(X^{(i)}|Y=y)$ stand for the y 'th output of the SimNet (ConvAC in log-space) realizing our model with parameters Θ . In the case of uniform class priors ($\mathbb{P}(Y=y) \equiv 1/K$), the empirical estimation of $\mathcal{L}(\Theta)$ may be written as:

$$\mathcal{L}(\Theta; S) = -\frac{1}{|S|} \sum_{i=1}^{|S|} \log \frac{e^{N_\Theta(X^{(i)}; Y^{(i)})}}{\sum_{y=1}^K e^{N_\Theta(X^{(i)}; y)}} - \frac{1}{|S|} \sum_{i=1}^{|S|} \log \sum_{y=1}^K e^{N_\Theta(X^{(i)}; y)} \quad (2)$$

This objective includes the standard softmax loss as its first term, and an additional generative loss as its second. Rather than employing dedicated Maximum Likelihood methods for training (e.g. Expectation Minimization), we leverage once more the resemblance between our networks and ConvNets, and optimize the above objective using Stochastic Gradient Descent (SGD).

3 Classification under Missing Data through Marginalization

A major advantage of generative models over discriminative ones lies in their ability to cope with missing data, specifically in the context of classification. By and large, discriminative methods either attempt to complete missing parts of the data before classification (a process known as *data imputation*), or learn directly to classify data with missing values [28]. The first of these approaches relies on the quality of data completion, a much more difficult task than the original one of classification under missing data. Even if the completion was optimal, the resulting classifier is known to be sub-optimal (see app. E). The second approach does not rely on data completion, but nonetheless assumes that the distribution of missing values at train and test times are similar, a condition which often does not hold in practice. Indeed, Globerson and Roweis [17] coined the term ‘‘nightmare at test time’’ to refer to the common situation where a classifier must cope with missing data whose distribution is different from that encountered in training.

As opposed to discriminative methods, generative models are endowed with a natural mechanism for classification under missing data. Namely, a generative model can simply marginalize over missing values, effectively classifying under all possible completions, weighing each completion according to its probability. This, however, requires tractable inference and marginalization. We have already shown in sec. 2 that TMMs support the former, and will show in sec. F that marginalization can be just as efficient. Beforehand, we lay out the formulation of classification under missing data.

Let \mathcal{X} be a random vector in \mathbb{R}^s representing an object, and let \mathcal{Y} be a random variable in $[K]$ representing its label. Denote by $\mathcal{D}(\mathcal{X}, \mathcal{Y})$ the joint distribution of $(\mathcal{X}, \mathcal{Y})$, and by $(\mathbf{x} \in \mathbb{R}^s, y \in [K])$ specific realizations thereof. Assume that after sampling a specific instance (\mathbf{x}, y) , a random binary vector \mathcal{M} is drawn conditioned on $\mathcal{X}=\mathbf{x}$. More concretely, we sample a binary mask $\mathbf{m} \in \{0, 1\}^s$ (realization of \mathcal{M}) according to a distribution $\mathcal{Q}(\cdot|\mathcal{X}=\mathbf{x})$. x_i is considered missing if m_i is equal to zero, and observed otherwise. Formally, we consider the vector $\mathbf{x} \odot \mathbf{m}$, whose i 'th coordinate is defined to hold x_i if $m_i=1$, and the wildcard $*$ if $m_i=0$. The classification task is then to predict y given access solely to $\mathbf{x} \odot \mathbf{m}$.

Following the works of Rubin [36], Little and Rubin [28], we consider three cases for the missingness distribution $\mathcal{Q}(\mathcal{M}=\mathbf{m}|\mathcal{X}=\mathbf{x})$: missing completely at random (*MCAR*), where \mathcal{M} is independent of \mathcal{X} , i.e. $\mathcal{Q}(\mathcal{M}=\mathbf{m}|\mathcal{X}=\mathbf{x})$ is a function of \mathbf{m} but not of \mathbf{x} ; missing at random (*MAR*), where \mathcal{M} is independent of the missing values in \mathcal{X} , i.e. $\mathcal{Q}(\mathcal{M}=\mathbf{m}|\mathcal{X}=\mathbf{x})$ is a function of both \mathbf{m} and \mathbf{x} , but is not affected by changes in x_i if $m_i=0$; and missing not at random (*MNAR*), covering the rest of the distributions for which \mathcal{M} depends on missing values in \mathcal{X} , i.e. $\mathcal{Q}(\mathcal{M}=\mathbf{m}|\mathcal{X}=\mathbf{x})$ is a function of both \mathbf{m} and \mathbf{x} , which at least sometimes is sensitive to changes in x_i when $m_i=0$.

Let \mathbb{P} be the joint distribution of the object \mathcal{X} , label \mathcal{Y} , and missingness mask \mathcal{M} :

$$\mathbb{P}(\mathcal{X}=\mathbf{x}, \mathcal{Y}=y, \mathcal{M}=\mathbf{m}) = \mathcal{D}(\mathcal{X}=\mathbf{x}, \mathcal{Y}=y) \cdot \mathcal{Q}(\mathcal{M}=\mathbf{m}|\mathcal{X}=\mathbf{x})$$

For given $\mathbf{x} \in \mathbb{R}^s$ and $\mathbf{m} \in \{0, 1\}^s$, denote by $o(\mathbf{x}, \mathbf{m})$ the event where the random vector \mathcal{X} coincides with \mathbf{x} on the coordinates i for which $m_i=1$. For example, if \mathbf{m} is an all-zero vector, $o(\mathbf{x}, \mathbf{m})$ covers the entire probability space, and if \mathbf{m} is an all-one vector, $o(\mathbf{x}, \mathbf{m})$ corresponds to the event $\mathcal{X}=\mathbf{x}$. With these notations in hand, we are now ready to characterize the optimal predictor in the presence of missing data. The proofs are common knowledge, but provided in app. E for completeness.

Claim 1. *For any data distribution \mathcal{D} and missingness distribution \mathcal{Q} , the optimal classification rule in terms of 0-1 loss is given by predicting the class $y \in [K]$, that maximizes $\mathbb{P}(\mathcal{Y}=y|o(\mathbf{x}, \mathbf{m})) \cdot \mathbb{P}(\mathcal{M}=\mathbf{m}|o(\mathbf{x}, \mathbf{m}), \mathcal{Y}=y)$, for an instance $\mathbf{x} \odot \mathbf{m}$.*

When the distribution \mathcal{Q} is MAR (or MCAR), the optimal classifier admits a simpler form, referred to as the *marginalized Bayes predictor*:

Corollary 1. *Under the conditions of claim 1, if the distribution \mathcal{Q} is MAR (or MCAR), the optimal classification rule may be written as:*

$$h^*(\mathbf{x} \odot \mathbf{m}) = \operatorname{argmax}_y \mathbb{P}(\mathcal{Y}=y|o(\mathbf{x}, \mathbf{m})) \quad (3)$$

Corollary 1 indicates that in the MAR setting, which is frequently encountered in practice, optimal classification does *not* require prior knowledge regarding the missingness distribution \mathcal{Q} . As long as one is able to realize the marginalized Bayes predictor (eq. 3), or equivalently, to compute the likelihoods of observed values conditioned on labels ($\mathbb{P}(o(\mathbf{x}, \mathbf{m})|Y=y)$), classification under missing data is guaranteed to be optimal, regardless of the corruption process taking place. This is in stark contrast to discriminative methods, which require access to the missingness distribution during training, and thus are not able to cope with unknown conditions at test time.

Most of this section dealt with the task of prediction given an input with missing data, where we assumed we had access to a “clean” training set, and only faced missingness during prediction. However, many times we wish to tackle the reverse task, where the training set itself is riddled with missing data. Tractability leads to an advantage here as well: under the MAR assumption, learning from missing data with the marginalized likelihood objective results in an unbiased classifier [28].

In the case of TMMs, marginalizing over missing values is just as efficient as plain inference – requires only a single pass through the corresponding network. The exact mechanism is carried out in similar fashion as in sum-product networks, and is covered in app. F. Accordingly, the marginalized Bayes predictor (eq. 3) is realized efficiently, and classification under missing data (in the MAR setting) is optimal (under generative assumption), regardless of the missingness distribution.

4 Related Works

There are many generative models realized through neural networks, and convolutional networks in particular, e.g. Generative Adversarial Networks [19], Variational Auto-Encoders [24], and NADE [38]. However, most do not possess tractable inference, and of the few that do, non possess tractable marginalization over any set of variables. Due to limits of space, we defer the discussion on the above to app. G, and in the remainder of this section focus instead on the most relevant works.

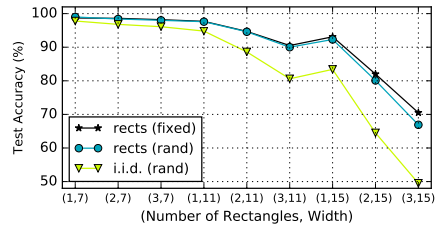
As mentioned in sec. 2, we build on the approach of specifying generative models through Arithmetic Circuits (ACs) [12], and specifically, our model is a strict subclass of the well-known Sum-Product Networks (SPNs) [34], under the decomposable and complete restrictions. Where our work differs is in our algebraic approach to eq. 1, which gives rise to a specific structure of ACs, called ConvACs, and a deep theory regarding their expressivity and inductive bias (see sec. 2.2). In contrast to the structure we proposed, the current literature on general SPNs does not prescribe any specific structures, and its theory is limited to either very specific instances [14], or very broad classes, e.g fixed-depth circuits [29]. In the early works on SPNs, specialized networks of complex structure were designed for each task based mainly on heuristics, often bearing little resemblance to common neural networks. Contemporary works have since moved on to focus mainly on learning the structure of SPNs directly from data [33, 16, 1, 35], leading to improved results in many domains. Despite that, only few published studies have applied this method to natural domains (images, audio, etc.), on which only limited performance, compared to other common methods, was reported, specifically on the MNIST dataset [1]. The above suggests that choosing the right architecture of general SPNs, at least on some domains, remains to be an unsolved problem. In addition, both the previously studied manually-designed SPNs, as well as ones with a learned structure, lead to models, which

n=	0	25	50	75	100	125	150
LP	97.9	97.5	96.4	94.1	89.2	80.9	70.2
HT-TMM	98.5	98.2	97.8	96.5	93.9	87.1	76.3

Table 1: Prediction for each two-class task of MNIST digits, under feature deletion noise.

$p_{\text{train}} \backslash p_{\text{test}}$	0.25	0.50	0.75	0.90	0.95	0.99
0.25	98.9	97.8	78.9	32.4	17.6	11.0
0.50	99.1	98.6	94.6	68.1	37.9	12.9
0.75	98.9	98.7	97.2	83.9	56.4	16.7
0.90	97.6	97.5	96.7	89.0	71.0	21.3
0.95	95.7	95.6	94.8	88.3	74.0	30.5
0.99	87.3	86.7	85.0	78.2	66.2	31.3
i.i.d. (rand)	98.7	98.4	97.0	87.6	70.6	29.6
rects (rand)	98.2	95.7	83.2	54.7	35.8	17.5

(a) MNIST with i.i.d. corruption



(b) MNIST with missing rectangles.

Figure 3: We examine ConvNets trained on one missingness distribution while tested on others. “(rand)” denotes training on distributions with randomized parameters. **(a)** i.i.d. corruption: trained with probability p_{train} and tested on p_{test} . **(b)** missing rectangles: training on randomized distributions (rand) compared to training on the same (fixed) missing rectangles distribution.

according to recent works on GPU-optimized algorithms [4], cannot be efficiently implemented due to their irregular memory access patterns. This is in stark contrast to our model, which leverages the same patterns as modern ConvNets, and thus enjoys similar run-time performance. An additional difference in our work is that we manage to successfully train our model using standard SGD. Even though this approach has already been considered by Poon and Domingos [34], they deemed it lacking and advocated for specialized optimization algorithms instead.

Outside the realm of generative networks, tractable graphical models, e.g. Latent Tree Models (LTMs) [30], are the most common method for tractable inference. Similar to SPNs, it is not straightforward to find the proper structure of graphical models for a particular problem, and most of the same arguments apply here as well. Nevertheless, it is noteworthy that recent progress in structure and parameters learning of LTMs [22, 3] was also brought forth by connections to tensor factorizations, similar to our approach. Unlike the aforementioned algorithms, we utilize tensor factorizations solely for deriving our model and analyzing its expressivity, while leaving learning to SGD – the most successful method for training neural networks. Leveraging their perspective to analyze the optimization properties of our model is viewed as a promising avenue for future research.

5 Experiments

We demonstrate the properties of TMMs through both qualitative and quantitative experiments. In sec. 5.1 we present state of the art results on image classification under missing data, with robustness to various missingness distributions. In sec. 5.2 we show that our results are not limited to images, by applying TMMs for speech recognition. Finally, in app. H we show visualizations of samples drawn from TMMs, shedding light on their generative nature. Our implementation, based on Caffe [23] and MAPS [4] (toolbox for efficient GPU code generation), as well as all other code for reproducing our experiments, are available at: <https://github.com/HUJI-Deep/Generative-ConvACs>. Extended details regarding the experiments are provided in app. I.

5.1 Image Classification under Missing Data

In this section we experiment on two datasets: MNIST [25] for digit classification, and small NORB [26] for 3D object recognition. In our results, we refer to models using shallow networks as CP-TMM, and to those using deep networks as HT-TMM, in accordance with the respective tensor factorizations (see sec. 2). The theory discussed in sec. 2.2 guided our exact choice of architectures. Namely, we used the fact [27] that the capacity to model either short- or long-range correlations in the input, is related to the number of channels in the beginning or end of a network, respectively. In MNIST, discriminating between digits has more to do with long-range correlations than the basic strokes digits are made of, hence we chose to start with few channels and end with many – layer

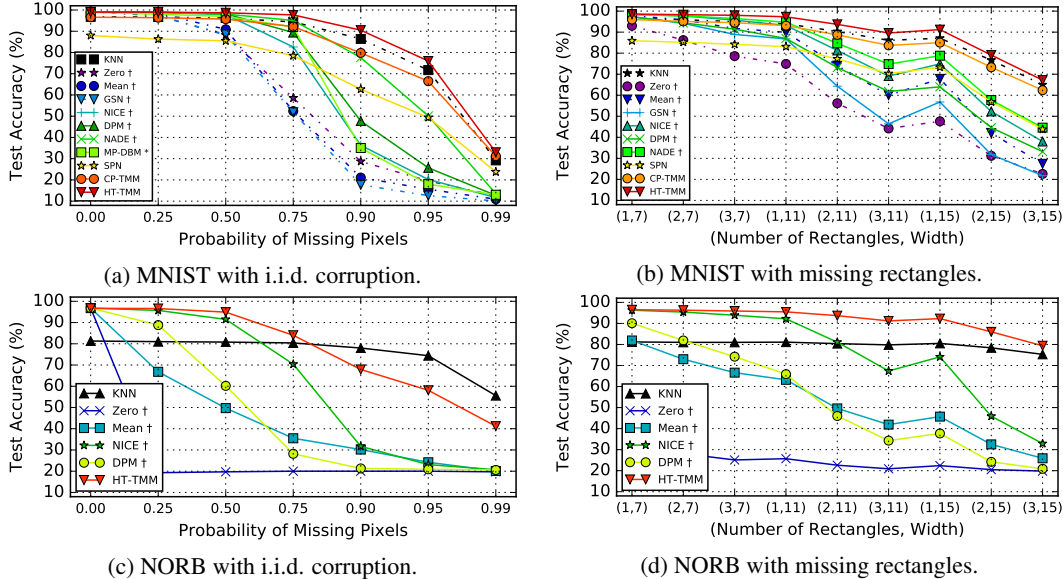


Figure 4: Blind classification under missing data. **(a,c)** Testing i.i.d. corruption with probability p for each pixel. **(b,d)** Testing missing rectangles corruption with n missing rectangles, each of width and height equal to W . (*) Based on the published results [18]. † Data imputation algorithms.

widths were set to 64-128-256-512. In contrast, the classes of NORB differ in much finer details, requiring more channels in the first layers, hence layer widths were set to 256-256-256-512. In both cases, $M = 32$ Gaussian mixing components were used.

We begin by comparing our generative approach to missing data against classical methods, namely, methods based on Globerson and Roweis [17]. They regard missing data as “feature deletion” noise, replace missing entries by zeros, and devise a learning algorithm over linear predictors that takes the number of missing features, n , into account. The method was later improved by Dekel and Shamir [13]. We compare TMMs to the latter, with n non-zero pixels randomly chosen and changed to zero, in the two-class prediction task derived from each pair of MNIST digits. Due to limits of their implementation, only 300 images per digit are used for training. Despite this, and the fact that the evaluated scenario is of the MNAR type (on which optimality is not guaranteed – see sec. 3), we achieve significantly better results (see table 1), and unlike their method, which requires several classifiers and knowing n , we use a single TMM with no prior knowledge.

Heading on to multi-class prediction under missing data, we focus on the challenging “blind” setting, where the missingness distribution at test time is completely unknown during training. We simulate two kinds of MAR missingness distributions: (i) an i.i.d. mask with a fixed probability $p \in [0, 1]$ of dropping each pixel, and (ii) a mask composed of the union of n (possibly overlapping) rectangles of width and height W , each positioned randomly in the image (uniform distribution). We first demonstrate that purely discriminative classifiers cannot generalize to all missingness distributions, by training the standard LeNet ConvNet [25] on one set of distributions and then testing it on others (see fig. 3). Next, we present our main results. We compare our model against three different approaches. First, as a baseline, we use K-Nearest Neighbors (KNN) to vote on the most likely class, augmented with an l^2 -metric that disregards missing coordinates. KNN actually scores better than most methods, but its missingness-aware distance metric prevents the common memory and runtime optimizations, making it impractical for real-world settings. Second, we test various data-imputation methods, ranging from simply filling missing pixels with zeros or their mean, to modern generative models suited to inpainting. Data imputation is followed by a ConvNet prediction on the completed image. In general, we find that this approach only works well when few pixels are missing. Finally, we test generative classifiers other than our model, including MP-DBM and SPN (sum-product networks). MP-DBM is notable for being limited to approximations, and its results show the importance of using exact inference instead. For SPN, we have augmented the model from Poon and Domingos [34] with a class variable Y , and trained it to maximize the joint probability $P(X, Y)$ using the code of Zhao et al. [41]. The inferior performance of SPN suggests

that the structure of TMMs, which are in fact a special case, is advantageous. Due to limitations of available public code and time, not all methods were tested on all datasets and distributions. See fig. 4 for the complete results.

To conclude, TMMs significantly outperform all other methods tested on image classification with missing data. Although they are a special case of SPNs, their particular structure appears to be more effective than ones existing in the literature. We attribute this superiority to the fact that their architectural design is backed by comprehensive theoretical studies (see sec. 2.2).

5.2 Speech Recognition under Missing Data

To demonstrate the versatility of TMMs, we also conducted limited experiments on the TIMIT speech recognition dataset, following the same protocols as in sec. 5.1. We trained a TMM and a standard ConvNet on 256ms windows of raw data at 16Hz sample rate to predict the phoneme at the center of a window. Both the TMM and the ConvNet reached 78% accuracy on the clean dataset, but when half of the audio is missing i.i.d., accuracy of the ConvNet with mean imputation drops to 34%, while the TMM remains at 63%. Utilizing common audio inpainting methods [2] only improves accuracy of the ConvNet to 48%, well below that of TMM.

6 Summary

This paper focuses on generative models which admit tractable inference and marginalization, capabilities that lie outside the realm of contemporary neural network-based generative methods. We build on prior works on tractable models based on arithmetic circuits and sum-product networks, and leverage concepts from tensor analysis to derive a sub-class of models we call Tensorial Mixture Models (TMMs). In contrast to existing methods, our algebraic approach leads to a comprehensive understanding of the relation between model structure and representational properties. In practice, utilizing this understanding for the design of TMMs has led to state of the art performance in classification under missing data. We are currently investigating several avenues for future research, including semi-supervised learning, and examining more intricate ConvAC architectures, such as the ones suggested by Cohen et al. [11]).

Acknowledgments

This work is supported by Intel grant ICRI-CI #9-2012-6133, by ISF Center grant 1790/12 and by the European Research Council (TheoryDL project). Nadav Cohen is supported by a Google Fellowship in Machine Learning.

References

- [1] Tameem Adel, David Balduzzi, and Ali Ghodsi. Learning the Structure of Sum-Product Networks via an SVD-based Algorithm. *UAI*, 2015.
- [2] A Adler, V Emiya, M G Jafari, and M Elad. Audio inpainting. *IEEE Trans. on Audio, Speech and Language Processing*, 20:922–932, March 2012.
- [3] Animashree Anandkumar, Rong Ge, Daniel Hsu, Sham M Kakade, and Matus Telgarsky. Tensor decompositions for learning latent variable models. *Journal of Machine Learning Research* (), 15(1):2773–2832, 2014.
- [4] Tal Ben-Nun, Ely Levy, Amnon Barak, and Eri Rubin. Memory Access Patterns: The Missing Piece of the Multi-GPU Puzzle. In *Proceedings of the International Conference for High Performance Computing, Networking, Storage and Analysis*, pages 19:1–19:12. ACM, 2015.
- [5] Yoshua Bengio, Éric Thibodeau-Laufer, Guillaume Alain, and Jason Yosinski. Deep Generative Stochastic Networks Trainable by Backprop. In *International Conference on Machine Learning*, 2014.
- [6] Richard Caron and Tim Traynor. The Zero Set of a Polynomial. *WSMR Report 05-02*, 2005.
- [7] Nadav Cohen and Amnon Shashua. SimNets: A Generalization of Convolutional Networks. In *Advances in Neural Information Processing Systems NIPS, Deep Learning Workshop*, 2014.

- [8] Nadav Cohen and Amnon Shashua. Inductive Bias of Deep Convolutional Networks through Pooling Geometry. In *International Conference on Learning Representations ICLR*, April 2017.
- [9] Nadav Cohen, Or Sharir, and Amnon Shashua. On the Expressive Power of Deep Learning: A Tensor Analysis. In *Conference on Learning Theory COLT*, May 2016.
- [10] Nadav Cohen, Or Sharir, and Amnon Shashua. Deep SimNets. In *Computer Vision and Pattern Recognition CVPR*, May 2016.
- [11] Nadav Cohen, Ronen Tamari, and Amnon Shashua. Boosting Dilated Convolutional Networks with Mixed Tensor Decompositions. *arXiv.org*, 2017.
- [12] Adnan Darwiche. A differential approach to inference in Bayesian networks. *Journal of the ACM (JACM)*, 50(3):280–305, May 2003.
- [13] Ofer Dekel and Ohad Shamir. Learning to classify with missing and corrupted features. In *International Conference on Machine Learning*. ACM, 2008.
- [14] Olivier Delalleau and Yoshua Bengio. Shallow vs. Deep Sum-Product Networks. *Advances in Neural Information Processing Systems*, pages 666–674, 2011.
- [15] Laurent Dinh, David Krueger, and Yoshua Bengio. NICE: Non-linear Independent Components Estimation. *arXiv.org*, October 2014.
- [16] R Gens and P M Domingos. Learning the Structure of Sum-Product Networks. *International Conference on Machine Learning*, 2013.
- [17] Amir Globerson and Sam Roweis. Nightmare at test time: robust learning by feature deletion. In *International Conference on Machine Learning*. ACM, 2006.
- [18] Ian Goodfellow, Mehdi Mirza, Aaron Courville, and Yoshua Bengio. Multi-Prediction Deep Boltzmann Machines. *Advances in Neural Information Processing Systems*, 2013.
- [19] Ian Goodfellow, Jean Pouget-Abadie, Mehdi Mirza, Bing Xu, David Warde-Farley, Sherjil Ozair, Aaron Courville, and Yoshua Bengio. Generative Adversarial Nets. *Advances in Neural Information Processing Systems*, 2014.
- [20] W Hackbusch and S Kühn. A New Scheme for the Tensor Representation. *Journal of Fourier Analysis and Applications*, 15(5):706–722, 2009.
- [21] Thomas Hofmann. *Probabilistic latent semantic analysis*. Morgan Kaufmann Publishers Inc., July 1999.
- [22] Furong Huang, Niranjan U N, Ioakeim Perros, Robert Chen, Jimeng Sun, and Anima Anandkumar. Scalable Latent Tree Model and its Application to Health Analytics. In *NIPS Machine Learning for Healthcare Workshop*, 2015.
- [23] Yangqing Jia, Evan Shelhamer, Jeff Donahue, Sergey Karayev, Jonathan Long, Ross B Girshick, Sergio Guadarrama, and Trevor Darrell. Caffe: Convolutional Architecture for Fast Feature Embedding. *CoRR abs/1202.2745*, cs.CV, 2014.
- [24] Diederik P Kingma and Max Welling. Auto-Encoding Variational Bayes. In *International Conference on Learning Representations*, 2014.
- [25] Yan LeCun, Leon Bottou, Yoshua Bengio, and Patrick Haffner. Gradient-based learning applied to document recognition. *Proceedings of the IEEE*, 86(11):2278–2324, 1998.
- [26] Yann LeCun, Fu Jie Huang, and Léon Bottou. Learning Methods for Generic Object Recognition with Invariance to Pose and Lighting. *Computer Vision and Pattern Recognition*, 2004.
- [27] Yoav Levine, David Yakira, Nadav Cohen, and Amnon Shashua. Deep Learning and Quantum Entanglement: Fundamental Connections with Implications to Network Design. *arXiv.org*, April 2017.
- [28] Roderick J A Little and Donald B Rubin. *Statistical analysis with missing data (2nd edition)*. John Wiley & Sons, Inc., September 2002.
- [29] James Martens and Venkatesh Medabalimi. On the Expressive Efficiency of Sum Product Networks. *CoRR abs/1202.2745*, cs.LG, 2014.
- [30] Raphaël Mourad, Christine Sinoquet, Nevin Lianwen Zhang, Tengfei Liu, and Philippe Leray. A Survey on Latent Tree Models and Applications. *J. Artif. Intell. Res.* (), cs.LG:157–203, 2013.

- [31] Andrew Y Ng and Michael I Jordan. On Discriminative vs. Generative Classifiers: A comparison of logistic regression and naive Bayes. In *Advances in Neural Information Processing Systems NIPS, Deep Learning Workshop*, 2002.
- [32] F Pedregosa, G Varoquaux, A Gramfort, V Michel, B Thirion, O Grisel, M Blondel, P Prettenhofer, R Weiss, V Dubourg, J Vanderplas, A Passos, D Cournapeau, M Brucher, M Perrot, and E Duchesnay. Scikit-learn: Machine Learning in Python. *Journal of Machine Learning Research* (), 12:2825–2830, 2011.
- [33] Robert Peharz, Bernhard C Geiger, and Franz Pernkopf. Greedy Part-Wise Learning of Sum-Product Networks. In *Machine Learning and Knowledge Discovery in Databases*, pages 612–627. Springer Berlin Heidelberg, Berlin, Heidelberg, September 2013.
- [34] Hoifung Poon and Pedro Domingos. Sum-Product Networks: A New Deep Architecture. In *Uncertainty in Artificial Intelligence*, 2011.
- [35] Amirmohammad Rooshenas and Daniel Lowd. Learning Sum-Product Networks with Direct and Indirect Variable Interactions. *ICML*, 2014.
- [36] Donald B Rubin. Inference and missing data. *Biometrika*, 63(3):581–592, December 1976.
- [37] Jascha Sohl-Dickstein, Eric A Weiss, Niru Maheswaranathan, and Surya Ganguli. Deep Unsupervised Learning using Nonequilibrium Thermodynamics. *International Conference on Machine Learning*, 2015.
- [38] Benigno Uria, Marc-Alexandre Côté, Karol Gregor, Iain Murray, and Hugo Larochelle. Neural Autoregressive Distribution Estimation. *Journal of Machine Learning Research* (), 17(205):1–37, 2016.
- [39] Aaron van den Oord, Nal Kalchbrenner, and Koray Kavukcuoglu. Pixel Recurrent Neural Networks. In *International Conference on Machine Learning*, 2016.
- [40] Matthew D Zeiler and Rob Fergus. Visualizing and Understanding Convolutional Networks. In *European Conference on Computer Vision*. Springer International Publishing, 2014.
- [41] Han Zhao, Pascal Poupart, and Geoff Gordon. A Unified Approach for Learning the Parameters of Sum-Product Networks. In *Advances in Neural Information Processing Systems NIPS, Deep Learning Workshop*, 2016.
- [42] Daniel Zoran and Yair Weiss. From learning models of natural image patches to whole image restoration. *ICCV*, pages 479–486, 2011.

A The Universality of Tensorial Mixture Models

In this section we prove the universality property of Generative ConvACs, as discussed in sec. 2. We begin by taking note from functional analysis and define a new property called *PDF total set*, which is similar in concept to a *total set*, followed by proving that this property is invariant under the cartesian product of functions, which entails the universality of these models as a corollary.

Definition 1. Let \mathcal{F} be a set of PDFs over \mathbb{R}^s . \mathcal{F} is PDF total iff for any PDF $h(\mathbf{x})$ over \mathbb{R}^s and for all $\epsilon > 0$ there exists $M \in \mathbb{N}$, $\{f_1(\mathbf{x}), \dots, f_M(\mathbf{x})\} \subset \mathcal{F}$ and $\mathbf{w} \in \Delta^{M-1}$ s.t. $\left\| h(\mathbf{x}) - \sum_{i=1}^M w_i f_i(\mathbf{x}) \right\|_1 < \epsilon$. In other words, a set is a PDF total set if its convex span is a dense set under L^1 norm.

Claim 2. Let \mathcal{F} be a set of PDFs over \mathbb{R}^s and let $\mathcal{F}^{\otimes N} = \{\prod_{i=1}^N f_i(\mathbf{x}) | \forall i, f_i(\mathbf{x}) \in \mathcal{F}\}$ be a set of PDFs over the product space $(\mathbb{R}^s)^N$. If \mathcal{F} is a PDF total set then $\mathcal{F}^{\otimes N}$ is PDF total set.

Proof. If \mathcal{F} is the set of Gaussian PDFs over \mathbb{R}^s with diagonal covariance matrices, which is known to be a PDF total set, then $\mathcal{F}^{\otimes N}$ is the set of Gaussian PDFs over $(\mathbb{R}^s)^N$ with diagonal covariance matrices and the claim is trivially true.

Otherwise, let $h(\mathbf{x}_1, \dots, \mathbf{x}_N)$ be a PDF over $(\mathbb{R}^s)^N$ and let $\epsilon > 0$. From the above, there exists $K \in \mathbb{N}$, $\mathbf{w} \in \Delta^{K-1}$ and a set of diagonal Gaussians $\{g_{ij}(\mathbf{x})\}_{i \in [M_1], j \in [N]}$ s.t.

$$\left\| g(\mathbf{x}) - \sum_{i=1}^{M_1} w_i \prod_{j=1}^N g_{ij}(\mathbf{x}_j) \right\|_1 < \frac{\epsilon}{2} \quad (4)$$

Additionally, since \mathcal{F} is a PDF total set then there exists $M_2 \in \mathbb{N}$, $\{f_k(\mathbf{x})\}_{k \in [M_2]} \subset \mathcal{F}$ and $\{\mathbf{w}_{ij} \in \Delta^{M_2-1}\}_{i \in [M_1], j \in [N]}$ s.t. for all $i \in [M_1], j \in [N]$ it holds that $\left\| g_{ij}(\mathbf{x}) - \sum_{k=1}^{M_2} w_{ijk} f_k(\mathbf{x}) \right\|_1 < \frac{\epsilon}{2N}$, from which it is trivially proven using a telescopic sum and the triangle inequality that:

$$\left\| \sum_{i=1}^{M_1} w_i \prod_{j=1}^N g_{ij}(\mathbf{x}) - \sum_{i=1}^{M_1} w_i \prod_{j=1}^N \sum_{k=1}^{M_2} w_{ijk} f_k(\mathbf{x}_j) \right\|_1 < \frac{\epsilon}{2} \quad (5)$$

From eq. 4, eq. 5 the triangle inequality it holds that:

$$\left\| g(\mathbf{x}) - \sum_{k_1, \dots, k_N=1}^{M_2} \mathcal{A}_{k_1, \dots, k_N} \prod_{j=1}^N f_{k_j}(\mathbf{x}_j) \right\|_1 < \epsilon$$

where $\mathcal{A}_{k_1, \dots, k_N} = \sum_{i=1}^{M_1} w_i \prod_{j=1}^N w_{ijk_j}$ which holds $\sum_{k_1, \dots, k_N=1}^{M_2} \mathcal{A}_{k_1, \dots, k_N} = 1$. Taking $M = M_2^N$, $\{\prod_{j=1}^N f_{k_j}(\mathbf{x}_j)\}_{k_1 \in [M_2], \dots, k_N \in [M_2]} \subset \mathcal{F}^{\otimes N}$ and $\mathbf{w} = \text{vec}(\mathcal{A})$ completes the proof. \square

Corollary 2. Let \mathcal{F} be a PDF total set of PDFs over \mathbb{R}^s , then the family of Generative ConvACs with mixture components from \mathcal{F} can approximate any PDF over $(\mathbb{R}^s)^N$ arbitrarily well, given arbitrarily many components.

B TMMs with Sparsity Constraints Can Represent Gaussian Mixture Models

As discussed in sec. 2, TMMs become tractable when a sparsity constraint is imposed on the priors tensor, i.e. most of the entries of the tensors are replaced with zeros. In this section, we demonstrate that under such a case, TMMs can represent Gaussian Mixture Models with diagonal covariance matrices, probably the most common type of mixture models.

With the same notations as sec. 2, assume the number of mixing components of the TMM is $M = N \cdot K$ for some $K \in \mathbb{N}$, let $\{\mathcal{N}(\mathbf{x}; \boldsymbol{\mu}_{ki}, \text{diag}(\boldsymbol{\sigma}_{ki}^2))\}_{k,i}^{K,N}$ be these components, and finally, assume the prior tensor has the following structure:

$$P(d_1, \dots, d_N) = \begin{cases} w_k & \forall i \in [N], d_i = N \cdot (k-1) + i \\ 0 & \text{Otherwise} \end{cases}$$

then eq. 1 reduces to:

$$P(X) = \sum_{k=1}^K w_k \prod_{i=1}^N \mathcal{N}(\mathbf{x}; \boldsymbol{\mu}_{ki}, \text{diag}(\boldsymbol{\sigma}_{ki}^2)) = \sum_{k=1}^K w_k \mathcal{N}(\mathbf{x}; \tilde{\boldsymbol{\mu}}_k, \text{diag}(\tilde{\boldsymbol{\sigma}}_k^2))$$

$$\tilde{\boldsymbol{\mu}}_k = (\boldsymbol{\mu}_{k1}^T, \dots, \boldsymbol{\mu}_{kN}^T)^T \quad \tilde{\boldsymbol{\sigma}}_k^2 = ((\boldsymbol{\sigma}_{k1}^2)^T, \dots, (\boldsymbol{\sigma}_{kN}^2)^T)^T$$

which is equivalent to a diagonal GMM with mixing weights $\mathbf{w} \in \Delta^{K-1}$ (where Δ^{K-1} is the K -dimensional simplex) and Gaussian mixture components with means $\{\tilde{\boldsymbol{\mu}}_k\}_{k=1}^K$ and covariances $\{\text{diag}(\tilde{\boldsymbol{\sigma}}_k^2)\}_{k=1}^K$.

C Background on Tensor Factorizations

In this section we establish the minimal background in the field of tensor analysis required for following our work. A tensor is best thought of as a multi-dimensional array $\mathcal{A}_{d_1, \dots, d_N} \in \mathbb{R}$, where $\forall i \in [N], d_i \in [M_i]$. The number of indexing entries in the array, which are also called *modes*, is referred to as the *order* of the tensor. The number of values an index of a particular mode can take is referred to as the *dimension* of the mode. The tensor $\mathcal{A} \in \mathbb{R}^{M_1 \otimes \dots \otimes M_N}$ mentioned above is thus of order N with dimension M_i in its i -th mode. For our purposes we typically assume that $M_1 = \dots = M_N = M$, and simply denote it as $\mathcal{A} \in (\mathbb{R}^M)^{\otimes N}$.

The fundamental operator in tensor analysis is the *tensor product*. The tensor product operator, denoted by \otimes , is a generalization of outer product of vectors (1-ordered vectors) to any pair of tensors. Specifically, let \mathcal{A} and \mathcal{B} be tensors of order P and Q respectively, then the tensor product $\mathcal{A} \otimes \mathcal{B}$ results in a tensor of order $P + Q$, defined by: $(\mathcal{A} \otimes \mathcal{B})_{d_1, \dots, d_{P+Q}} = \mathcal{A}_{d_1, \dots, d_P} \cdot \mathcal{B}_{d_{P+1}, \dots, d_{P+Q}}$.

The main concept from tensor analysis we use in our work is that of tensor decompositions. The most straightforward and common tensor decomposition format is the rank-1 decomposition, also known as a CANDECOMP/PARAFAC decomposition, or in short, a *CP decomposition*. The CP decomposition is a natural extension of low-rank matrix decomposition to general tensors, both built upon the concept of a linear combination of rank-1 elements. Similarly to matrices, tensors of the form $\mathbf{v}^{(1)} \otimes \dots \otimes \mathbf{v}^{(N)}$, where $\mathbf{v}^{(i)} \in \mathbb{R}^{M_i}$ are non-zero vectors, are regarded as N -ordered rank-1 tensors, thus the rank- Z CP decomposition of a tensor \mathcal{A} is naturally defined by:

$$\begin{aligned} \mathcal{A} &= \sum_{z=1}^Z a_z \mathbf{a}^{z,1} \otimes \dots \otimes \mathbf{a}^{z,N} \\ \Rightarrow \mathcal{A}_{d_1, \dots, d_N} &= \sum_{z=1}^Z a_z \prod_{i=1}^N a_{d_i}^{z,i} \end{aligned} \quad (6)$$

where $\{\mathbf{a}^{z,i} \in \mathbb{R}^{M_i}\}_{i=1, z=1}^{N,Z}$ and $\mathbf{a} \in \mathbb{R}^Z$ are the parameters of the decomposition. As mentioned above, for $N = 2$ it is equivalent to low-order matrix factorization. It is simple to show that any tensor \mathcal{A} can be represented by the CP decomposition for some Z , where the minimal such Z is known as its *tensor rank*.

Another decomposition we will use in this paper is of a hierarchical nature and known as the Hierarchical Tucker decomposition [20], which we will refer to as *HT decomposition*. While the CP decomposition combines vectors into higher order tensors in a single step, the HT decomposition does that more gradually, combining vectors into matrices, these matrices into 4th ordered tensors and so on recursively in a hierarchically fashion. Specifically, the following describes the recursive formula of the HT decomposition⁴ for a tensor $\mathcal{A} \in (\mathbb{R}^M)^{\otimes N}$ where $N = 2^L$, i.e. N is a power of two⁵:

$$\begin{aligned} \phi^{1,j,\gamma} &= \sum_{\alpha=1}^{r_0} a_{\alpha}^{1,j,\gamma} \mathbf{a}^{0,2j-1,\alpha} \otimes \mathbf{a}^{0,2j,\alpha} \\ &\dots \\ \phi^{l,j,\gamma} &= \sum_{\alpha=1}^{r_{l-1}} a_{\alpha}^{l,j,\gamma} \underbrace{\phi^{l-1,2j-1,\alpha}}_{\text{order } 2^{l-1}} \otimes \underbrace{\phi^{l-1,2j,\alpha}}_{\text{order } 2^{l-1}} \\ &\dots \\ \phi^{L-1,j,\gamma} &= \sum_{\alpha=1}^{r_{L-2}} a_{\alpha}^{L-1,j,\gamma} \underbrace{\phi^{L-2,2j-1,\alpha}}_{\text{order } \frac{N}{4}} \otimes \underbrace{\phi^{L-2,2j,\alpha}}_{\text{order } \frac{N}{4}} \\ \mathcal{A} &= \sum_{\alpha=1}^{r_{L-1}} a_{\alpha}^L \underbrace{\phi^{L-1,1,\alpha}}_{\text{order } \frac{N}{2}} \otimes \underbrace{\phi^{L-1,2,\alpha}}_{\text{order } \frac{N}{2}} \end{aligned} \quad (7)$$

where the parameters of the decomposition are the vectors $\{\mathbf{a}^{l,j,\gamma} \in \mathbb{R}^{r_{l-1}}\}_{l \in \{0, \dots, L-1\}, j \in [N/2^l], \gamma \in [r_l]}$ and the top level vector $\mathbf{a}^L \in \mathbb{R}^{r_{L-1}}$, and the scalars $r_0, \dots, r_{L-1} \in \mathbb{N}$ are referred to as the *ranks of the decomposition*. Similar to the CP decomposition, any tensor can be represented by an HT decomposition. Moreover,

⁴ More precisely, we use a special case of the canonical HT decomposition as presented in Hackbusch and Kühn [20]. In the terminology of the latter, the matrices $A^{l,j,\gamma}$ are diagonal and equal to $\text{diag}(\mathbf{a}^{l,j,\gamma})$ (using the notations from eq. 7).

⁵The requirement for N to be a power of two is solely for simplifying the definition of the HT decomposition. More generally, instead of defining it through a complete binary tree describing the order of operations, the canonical decomposition can use any balanced binary tree.

any given CP decomposition can be converted to an HT decomposition by only a polynomial increase in the number of parameters.

Finally, since we are dealing with generative models, the tensors we study are non-negative and sum to one, i.e. the vectorization of \mathcal{A} (rearranging its entries to the shape of a vector), denoted by $\text{vec}(\mathcal{A})$, is constrained to lie in the multi-dimensional simplex, denoted by:

$$\Delta^k := \left\{ \mathbf{x} \in \mathbb{R}^{k+1} \mid \sum_{i=1}^{k+1} x_i = 1, \forall i \in [k+1] : x_i \geq 0 \right\} \quad (8)$$

D Proof for the Depth Efficiency of Convolutional Arithmetic Circuits with Simplex Constraints

In this section we prove that the depth efficiency property of ConvACs that was proved in Cohen et al. [9] applies also to the generative variant of ConvACs we have introduced in sec. 2. Our analysis relies on basic knowledge of tensor analysis and its relation to ConvACs, specifically, that the concept of “ranks” of each factorization scheme is equivalent to the number of channels in these networks. For completeness, we provide a short introduction to tensor analysis in app. C. The

We prove the following theorem, which is the generative analog of theorem 1 from [9]:

Theorem 1. *Let \mathcal{A}^y be a tensor of order N and dimension M in each mode, generated by the recursive formulas in eq. 7, under the simplex constraints introduced in sec. 2. Define $r := \min\{r_0, M\}$, and consider the space of all possible configurations for the parameters of the decomposition $\{\mathbf{a}^{l,j,\gamma} \in \Delta^{r_{l-1}-1}\}_{l,j,\gamma}$. In this space, the generated tensor \mathcal{A}^y will have CP-rank of at least $r^{N/2}$ almost everywhere (w.r.t. the product measure of simplex spaces). Put differently, the configurations for which the CP-rank of \mathcal{A}^y is less than $r^{N/2}$ form a set of measure zero. The exact same result holds if we constrain the composition to be “shared”, i.e. set $\mathbf{a}^{l,j,\gamma} \equiv \mathbf{a}^{l,\gamma}$ and consider the space of $\{\mathbf{a}^{l,\gamma} \in \Delta^{r_{l-1}-1}\}_{l,\gamma}$ configurations.*

The only differences between ConvACs and their generative counter-parts are the simplex constraints applied to the parameters of the models, which necessitate a careful treatment to the measure theoretical arguments of the original proof. More specifically, while the k -dimensional simplex Δ^k is a subset of the $k+1$ -dimensional space \mathbb{R}^{k+1} , it has a zero measure with respect to the Lebesgue measure over \mathbb{R}^{k+1} . The standard method to define a measure over Δ^k is by the Lebesgue measure over \mathbb{R}^k of its projection to that space, i.e. let $\lambda : \mathbb{R}^k \rightarrow \mathbb{R}$ be the Lebesgue measure over \mathbb{R}^k , $p : \mathbb{R}^{k+1} \rightarrow \mathbb{R}^k, p(\mathbf{x}) = (x_1, \dots, x_k)^T$ be a projection, and $A \subset \Delta^k$ be a subset of the simplex, then the latter’s measure is defined as $\lambda(p(A))$. Notice that $p(\Delta^k)$ has a positive measure, and moreover that p is invertible over the set $p(\Delta^k)$, and that its inverse is given by $p^{-1}(x_1, \dots, x_k) = (x_1, \dots, x_k, 1 - \sum_{i=1}^k x_i)$. In our case, the parameter space is the cartesian product of several simplex spaces of different dimensions, for each of them the measure is defined as above, and the measure over their cartesian product is uniquely defined by the product measure. Though standard, the choice of the projection function p above could be seen as a limitation, however, the set of zero measure sets in Δ^k is identical for any reasonable choice of a projection π (e.g. all polynomial mappings). More specifically, for any projection $\pi : \mathbb{R}^{k+1} \rightarrow \mathbb{R}^k$ that is invertible over $\pi(\Delta^k)$, π^{-1} is differentiable, and the Jacobian of π^{-1} is bounded over $\pi(\Delta^k)$, then a subset $A \subset \Delta^k$ is of measure zero w.r.t. the projection π iff it is of measure zero w.r.t. p (as defined above). This implies that if we sample the weights of the generative decomposition (eq. 7 with simplex constraints) by a continuous distribution, a property that holds with probability 1 under the standard parameterization (projection p), will hold with probability 1 under any reasonable parameterization.

We now state and prove a lemma that will be needed for our proof of theorem 1.

Lemma 1. *Let $M, N, K \in \mathbb{N}, 1 \leq r \leq \min\{M, N\}$ and a polynomial mapping $A : \mathbb{R}^K \rightarrow \mathbb{R}^{M \times N}$ (i.e. for every $i \in [M], j \in [N]$ then $A_{ij} : \mathbb{R}^K \rightarrow \mathbb{R}$ is a polynomial function). If there exists a point $\mathbf{x} \in \mathbb{R}^K$ s.t. $\text{rank}(A(\mathbf{x})) \geq r$, then the set $\{\mathbf{x} \in \mathbb{R}^K \mid \text{rank}(A(\mathbf{x})) < r\}$ has zero measure.*

Proof. Remember that $\text{rank}(A(\mathbf{x})) \geq r$ iff there exists a non-zero $r \times r$ minor of $A(\mathbf{x})$, which is polynomial in the entries of $A(\mathbf{x})$, and so it is polynomial in \mathbf{x} as well. Let $c = \binom{M}{r} \cdot \binom{N}{r}$ be the number of minors in A , denote the minors by $\{f_i(\mathbf{x})\}_{i=1}^c$, and define the polynomial function $f(\mathbf{x}) = \sum_{i=1}^c f_i(\mathbf{x})^2$. It thus holds that $f(\mathbf{x}) = 0$ iff for all $i \in [c]$ it holds that $f_i(\mathbf{x}) = 0$, i.e. $f(\mathbf{x}) = 0$ iff $\text{rank}(A(\mathbf{x})) < r$.

Now, $f(\mathbf{x})$ is a polynomial in the entries of \mathbf{x} , and so it either vanishes on a set of zero measure, or it is the zero polynomial (see Caron and Traynor [6] for proof). Since we assumed that there exists $\mathbf{x} \in \mathbb{R}^K$ s.t. $\text{rank}(A(\mathbf{x})) \geq r$, the latter option is not possible. \square

Following the work of Cohen et al. [9], our main proof relies on following notations and facts:

- We denote by $[\mathcal{A}]$ the matricization of an N -order tensor \mathcal{A} (for simplicity, N is assumed to be even), where rows and columns correspond to odd and even modes, respectively. Specifically, if $\mathcal{A} \in \mathbb{R}^{M_1 \times \dots \times M_N}$, the matrix $[\mathcal{A}]$ has $M_1 \cdot M_3 \cdot \dots \cdot M_{N-1}$ rows and $M_2 \cdot M_4 \cdot \dots \cdot M_N$ columns, rearranging the entries of the tensor such that $\mathcal{A}_{d_1, \dots, d_N}$ is stored in row index $1 + \sum_{i=1}^{N/2} (d_{2i-1} - 1) \prod_{j=i+1}^{N/2} M_{2j-1}$ and column index $1 + \sum_{i=1}^{N/2} (d_{2i} - 1) \prod_{j=i+1}^{N/2} M_{2j}$. Additionally, the matricization is a linear operator, i.e. for all scalars α_1, α_2 and tensors $\mathcal{A}_1, \mathcal{A}_2$ with the order and dimensions in every mode, it holds that $[\alpha_1 \mathcal{A}_1 + \alpha_2 \mathcal{A}_2] = \alpha_1 [\mathcal{A}_1] + \alpha_2 [\mathcal{A}_2]$.
- The relation between the Kronecker product (denoted by \odot) and the tensor product (denoted by \otimes) is given by $[\mathcal{A} \otimes \mathcal{B}] = [\mathcal{A}] \odot [\mathcal{B}]$.
- For any two matrices A and B , it holds that $\text{rank}(A \odot B) = \text{rank}(A) \cdot \text{rank}(B)$.
- Let Z be the CP-rank of \mathcal{A} , then it holds that $\text{rank}([\mathcal{A}]) \leq Z$ (see [9] for proof).

Proof of theorem 1. Stemming from the above stated facts, to show that the CP-rank of \mathcal{A}^y is at least $r^{N/2}$, it is sufficient to examine its matricization $[\mathcal{A}^y]$ and prove that $\text{rank}([\mathcal{A}^y]) \geq r^{N/2}$.

Notice from the construction of $[\mathcal{A}^y]$, according to the recursive formula of the HT-decomposition, that its entries are polynomial in the parameters of the decomposition, its dimensions are $M^{N/2}$ each and that $1 \leq r^{N/2} \leq M^{N/2}$. In accordance with the discussion on the measure of simplex spaces, for each vector parameter $\mathbf{a}^{l,j,\gamma} \in \Delta^{r_{l-1}-1}$, we instead examine its projection $\tilde{\mathbf{a}}^{l,j,\gamma} = p(\mathbf{a}^{l,j,\gamma}) \in \mathbb{R}^{r_{l-1}-1}$, and notice that $p^{-1}(\tilde{\mathbf{a}}^{l,j,\gamma})$ is a polynomial mapping⁶ w.r.t. $\tilde{\mathbf{a}}^{l,j,\gamma}$. Thus, $[\mathcal{A}^y]$ is a polynomial mapping w.r.t. the projected parameters $\{\tilde{\mathbf{a}}^{l,j,\gamma}\}_{l,j,\gamma}$, and using lemma 1 it is sufficient to show that there exists a set of parameters for which $\text{rank}([\mathcal{A}^y]) \geq r^{N/2}$.

Denoting for convenience $\phi^{L,1,1} := \mathcal{A}^y$ and $r_L = 1$, we will construct by induction over $l = 1, \dots, L$ a set of parameters, $\{\mathbf{a}^{l,j,\gamma}\}_{l,j,\gamma}$, for which the ranks of the matrices $\{[\phi^{l,j,\gamma}]\}_{j \in [N/2^l], \gamma \in [r_l]}$ are at least $r^{2^l/2}$, while enforcing the simplex constraints on the parameters. More so, we'll construct these parameters s.t. $\mathbf{a}^{l,j,\gamma} = \mathbf{a}^{l,\gamma}$, thus proving both the "unshared" and "shared" cases.

For the case $l = 1$ we have:

$$\phi^{1,j,\gamma} = \sum_{\alpha=1}^{r_0} a_{\alpha}^{1,j,\gamma} \mathbf{a}^{0,2j-1,\alpha} \otimes \mathbf{a}^{0,2j,\alpha}$$

and let $a_{\alpha}^{1,j,\gamma} = \frac{1_{\alpha \leq r}}{r}$ and $a_i^{0,j,\alpha} = 1_{\alpha=i}$ for all i, j, γ and $\alpha \leq M$, and $a_i^{0,j,\alpha} = 1_{i=1}$ for all i and $\alpha > M$, and so

$$[\phi^{1,j,\gamma}]_{i,j} = \begin{cases} 1/r & i = j \wedge i \leq r \\ 0 & \text{Otherwise} \end{cases}$$

which means $\text{rank}([\phi^{1,j,\gamma}]) = r$, while preserving the simplex constraints, which proves our inductive hypothesis for $l = 1$.

Assume now that $\text{rank}([\phi^{l-1,j',\gamma'}]) \geq r^{2^{l-1}/2}$ for all $j' \in [N/2^{l-1}]$ and $\gamma' \in [r_{l-1}]$. For some specific choice of $j \in [N/2^l]$ and $\gamma \in [r_l]$ we have:

$$\begin{aligned} \phi^{l,j,\gamma} &= \sum_{\alpha=1}^{r_{l-1}} a_{\alpha}^{l,j,\gamma} \phi^{l-1,2j-1,\alpha} \otimes \phi^{l-1,2j,\alpha} \\ \implies [\phi^{l,j,\gamma}] &= \sum_{\alpha=1}^{r_{l-1}} a_{\alpha}^{l,j,\gamma} [\phi^{l-1,2j-1,\alpha}] \odot [\phi^{l-1,2j,\alpha}] \end{aligned}$$

Denote $M_{\alpha} := [\phi^{l-1,2j-1,\alpha}] \odot [\phi^{l-1,2j,\alpha}]$ for $\alpha = 1, \dots, r_{l-1}$. By our inductive assumption, and by the general property $\text{rank}(A \odot B) = \text{rank}(A) \cdot \text{rank}(B)$, we have that the ranks of all matrices M_{α} are at least $r^{2^{l-1}/2} \cdot r^{2^{l-1}/2} = r^{2^l/2}$. Writing $[\phi^{l,j,\gamma}] = \sum_{\alpha=1}^{r_{l-1}} a_{\alpha}^{l,j,\gamma} \cdot M_{\alpha}$, and noticing that $\{M_{\alpha}\}$ do not depend on $\mathbf{a}^{l,j,\gamma}$, we simply pick $a_{\alpha}^{l,j,\gamma} = 1_{\alpha=1}$, and thus $\phi^{l,j,\gamma} = M_1$, which is of rank $r^{2^l/2}$. This completes the proof of the theorem. \square

From the perspective of ConvACs with simplex constraints, theorem 1 leads to the following corollary:

⁶As we mentioned earlier, p is invertible only over $p(\Delta^k)$, for which its inverse is given by $p^{-1}(x_1, \dots, x_k) = (x_1, \dots, x_k, 1 - \sum_{i=1}^k x_i)$. However, to simplify the proof and notations, we use p^{-1} as defined here over the entire range \mathbb{R}^{k-1} , even where it does not serve as the inverse of p .

Corollary 3. Assume the mixing components $\mathcal{M} = \{f_i(\mathbf{x}) \in L^2(\mathbb{R}^2) \cap L^1(\mathbb{R}^s)\}_{i=1}^M$ are square integrable⁷ probability density functions, which form a linearly independent set. Consider a deep ConvAC model with simplex constraints of polynomial size whose parameters are drawn at random by some continuous distribution. Then, with probability 1, the distribution realized by this network requires an exponential size in order to be realized (or approximated w.r.t. the L^2 distance) by the shallow ConvAC model with simplex constraints. The claim holds regardless of whether the parameters of the deep model are shared or not.

Proof. Given a coefficient tensor \mathcal{A} , the CP-rank of \mathcal{A} is a lower bound on the number of channels (of its next to last layer) required to represent that tensor by the ConvAC following the CP factorization. Additionally, since the mixing components are linearly independent, their products $\{\prod_{i=1}^N f_i(\mathbf{x}_i) | f_i \in \mathcal{M}\}$ are linearly independent as well, which entails that any distribution representable by the generative variant of ConvAC with mixing components \mathcal{M} has a unique coefficient tensor \mathcal{A} . From theorem 1, the set of parameters of a deep ConvAC model (under the simplex constraints) with a coefficient tensor of a polynomial CP-rank – the requirement for a polynomially-sized shallow ConvAC model with simplex constraints realizing that same distribution exactly – forms a set of measure zero.

It is left to prove, that not only is it impossible to exactly represent a distribution with an exponential coefficient tensor by a shallow model, it is also impossible to approximate it. This follows directly from lemma 7 in appendix B of Cohen et al. [9], as our case meets the requirement of that lemma. \square

E Proof for the Optimality of Marginalized Bayes Predictor

In this section we give short proofs for the claims from sec. 3, on the optimality of the marginalized Bayes predictor under missing-at-random (MAR) distribution, when the missingness mechanism is unknown, as well as the general case when we do not add additional assumptions. In addition, we will also present a counter example proving data imputation results lead to suboptimal classification performance. We begin by introducing several notations that augment the notations already introduced in the body of the article.

Given a specific mask realization $\mathbf{m} \in \{0, 1\}^s$, we use the following notations to denote partial assignments to the random vector \mathcal{X} . For the observed indices of \mathcal{X} , i.e. the indices for which $m_i = 1$, we denote a partial assignment by $\mathcal{X} \setminus \mathbf{m} = \mathbf{x}_o$, where $\mathbf{x}_o \in \mathbb{R}^{d_o}$ is a vector of length d_o equal to the number of observed indices. Similarly, we denote by $\mathcal{X} \cap \mathbf{m} = \mathbf{x}_m$ a partial assignment to the missing indices according to \mathbf{m} , where $\mathbf{x}_m \in \mathbb{R}^{d_m}$ is a vector of length d_m equal to the number of missing indices. As an example of the notation, for given realizations $\mathbf{x} \in \mathbb{R}^s$ and $\mathbf{m} \in \{0, 1\}^s$, we defined in sec. 3 the event $o(\mathbf{x}, \mathbf{m})$, which using current notation is marked by the partial assignment $\mathcal{X} \setminus \mathbf{m} = \mathbf{x}_o$ where \mathbf{x}_o matches the observed values of the vector \mathbf{x} according to \mathbf{m} .

With the above notations in place, we move on to prove claim 1, which describes the general solution to the optimal prediction rule given both the data and missingness distributions, and without adding any additional assumptions.

⁷It is important to note that most commonly used distribution functions are square integrable, e.g. most members of the exponential family such as the Gaussian distribution.

Proof of claim 1. Fix an arbitrary prediction rule h . We will show that $L(h^*) \leq L(h)$, where L is the expected 0-1 loss.

$$\begin{aligned}
1 - L(h) &= E_{(\mathbf{x}, \mathbf{m}, y) \sim (\mathcal{X}, \mathcal{M}, \mathcal{Y})} [1_{h(\mathbf{x} \odot \mathbf{m})=y}] \\
&= \sum_{\mathbf{m} \in \{0,1\}^s} \sum_{y \in [k]} \int_{\mathbb{R}^s} \mathbb{P}(\mathcal{M}=\mathbf{m}, \mathcal{X}=\mathbf{x}, \mathcal{Y}=y) 1_{h(\mathbf{x} \odot \mathbf{m})=y} d\mathbf{x} \\
&= \sum_{\mathbf{m} \in \{0,1\}^s} \sum_{y \in [k]} \int_{\mathbb{R}^{d_o}} \int_{\mathbb{R}^{d_m}} \\
&\quad \mathbb{P}(\mathcal{M}=\mathbf{m}, \mathcal{X} \setminus \mathbf{m}=\mathbf{x}_o, \mathcal{X} \cap \mathbf{m}=\mathbf{x}_m, \mathcal{Y}=y) 1_{h(\mathbf{x} \odot \mathbf{m})=y} d\mathbf{x}_o d\mathbf{x}_m \\
&= 1 \sum_{\mathbf{m} \in \{0,1\}^s} \sum_{y \in [k]} \int_{\mathbb{R}^{d_o}} 1_{h(\mathbf{x} \odot \mathbf{m})=y} d\mathbf{x}_o \\
&\quad \int_{\mathbb{R}^{d_m}} \mathbb{P}(\mathcal{M}=\mathbf{m}, \mathcal{X} \setminus \mathbf{m}=\mathbf{x}_o, \mathcal{X} \cap \mathbf{m}=\mathbf{x}_m, \mathcal{Y}=y) d\mathbf{x}_m \\
&= 2 \sum_{\mathbf{m} \in \{0,1\}^s} \sum_{y \in [k]} \int_{\mathbb{R}^{d_o}} 1_{h(\mathbf{x} \odot \mathbf{m})=y} \mathbb{P}(\mathcal{M}=\mathbf{m}, \mathcal{X} \setminus \mathbf{m}=\mathbf{x}_o, \mathcal{Y}=y) d\mathbf{x}_o \\
&= 3 \sum_{\mathbf{m} \in \{0,1\}^s} \int_{\mathbb{R}^{d_o}} \mathbb{P}(\mathcal{X} \setminus \mathbf{m}=\mathbf{x}_o) \sum_{y \in [k]} 1_{h(\mathbf{x} \odot \mathbf{m})=y} \mathbb{P}(\mathcal{Y}=y | \mathcal{X} \setminus \mathbf{m}=\mathbf{x}_o) \\
&\quad \mathbb{P}(\mathcal{M}=\mathbf{m} | \mathcal{X} \setminus \mathbf{m}=\mathbf{x}_o, \mathcal{Y}=y) d\mathbf{x}_o \\
&\leq 4 \sum_{\mathbf{m} \in \{0,1\}^s} \int_{\mathbb{R}^{d_o}} \mathbb{P}(\mathcal{X} \setminus \mathbf{m}=\mathbf{x}_o) \sum_{y \in [k]} 1_{h^*(\mathbf{x} \odot \mathbf{m})=y} \mathbb{P}(\mathcal{Y}=y | \mathcal{X} \setminus \mathbf{m}=\mathbf{x}_o) \\
&\quad \mathbb{P}(\mathcal{M}=\mathbf{m} | \mathcal{X} \setminus \mathbf{m}=\mathbf{x}_o, \mathcal{Y}=y) d\mathbf{x}_o \\
&= 1 - L(h^*)
\end{aligned}$$

Where (1) is because the output of $h(\mathbf{x} \odot \mathbf{m})$ is independent of the missing values, (2) by marginalization, (3) by conditional probability definition and (4) because by definition $h^*(\mathbf{x} \odot \mathbf{m})$ maximizes the expression $\mathbb{P}(\mathcal{Y}=y | \mathcal{X} \setminus \mathbf{m}=\mathbf{x}_o) \mathbb{P}(\mathcal{M}=\mathbf{m} | \mathcal{X} \setminus \mathbf{m}=\mathbf{x}_o, \mathcal{Y}=y)$ w.r.t. the possible values of y for fixed vectors \mathbf{m} and \mathbf{x}_o . Finally, by replacing integrals with sums, the proof holds exactly the same when instances (\mathcal{X}) are discrete. \square

We now continue and prove corollary 1, a direct implication of claim 1 which shows that in the MAR setting, the missingness distribution can be ignored, and the optimal prediction rule is given by the marginalized Bayes predictor.

Proof of corollary 1. Using the same notation as in the previous proof, and denoting by \mathbf{x}_o the partial vector containing the observed values of $\mathbf{x} \odot \mathbf{m}$, the following holds:

$$\begin{aligned}
&\mathbb{P}(\mathcal{M}=\mathbf{m} | o(\mathbf{x}, \mathbf{m}), \mathcal{Y}=y) := \mathbb{P}(\mathcal{M}=\mathbf{m} | \mathcal{X} \setminus \mathbf{m}=\mathbf{x}_o, \mathcal{Y}=y) \\
&= \int_{\mathbb{R}^{d_m}} \mathbb{P}(\mathcal{M}=\mathbf{m}, \mathcal{X} \cap \mathbf{m}=\mathbf{x}_m | \mathcal{X} \setminus \mathbf{m}=\mathbf{x}_o, \mathcal{Y}=y) d\mathbf{x}_m \\
&= \int_{\mathbb{R}^{d_m}} \mathbb{P}(\mathcal{X} \cap \mathbf{m}=\mathbf{x}_m | \mathcal{X} \setminus \mathbf{m}=\mathbf{x}_o, \mathcal{Y}=y) \\
&\quad \cdot \mathbb{P}(\mathcal{M}=\mathbf{m} | \mathcal{X} \cap \mathbf{m}=\mathbf{x}_m, \mathcal{X} \setminus \mathbf{m}=\mathbf{x}_o, \mathcal{Y}=y) d\mathbf{x}_m \\
&= 1 \int_{\mathbb{R}^{d_m}} \mathbb{P}(\mathcal{X} \cap \mathbf{m}=\mathbf{x}_m | \mathcal{X} \setminus \mathbf{m}=\mathbf{x}_o, \mathcal{Y}=y) \\
&\quad \cdot \mathbb{P}(\mathcal{M}=\mathbf{m} | \mathcal{X} \cap \mathbf{m}=\mathbf{x}_m, \mathcal{X} \setminus \mathbf{m}=\mathbf{x}_o) d\mathbf{x}_m \\
&= 2 \int_{\mathbb{R}^{d_m}} \mathbb{P}(\mathcal{X} \cap \mathbf{m}=\mathbf{x}_m | \mathcal{X} \setminus \mathbf{m}=\mathbf{x}_o, \mathcal{Y}=y) \cdot \mathbb{P}(\mathcal{M}=\mathbf{m} | \mathcal{X} \setminus \mathbf{m}=\mathbf{x}_o) d\mathbf{x}_m \\
&= \mathbb{P}(\mathcal{M}=\mathbf{m} | \mathcal{X} \setminus \mathbf{m}=\mathbf{x}_o) \int_{\mathbb{R}^{d_m}} \mathbb{P}(\mathcal{X} \cap \mathbf{m}=\mathbf{x}_m | \mathcal{X} \setminus \mathbf{m}=\mathbf{x}_o, \mathcal{Y}=y) d\mathbf{x}_m \\
&= \mathbb{P}(\mathcal{M}=\mathbf{m} | o(\mathbf{x}, \mathbf{m}))
\end{aligned}$$

Where (1) is due to the independence assumption of the events $\mathcal{Y} = y$ and $\mathcal{M} = \mathbf{m}$ conditioned on $\mathcal{X} = \mathbf{x}$, while noting that $(\mathcal{X} \setminus \mathbf{m} = \mathbf{x}_o) \wedge (\mathcal{X} \cap \mathbf{m} = \mathbf{x}_m)$ is a complete assignment of \mathcal{X} . (2) is due to the MAR assumption, i.e. that for a given \mathbf{m} and \mathbf{x}_o it holds for all $\mathbf{x}_m \in \mathbb{R}^{d_m}$:

$$\mathbb{P}(\mathcal{M}=\mathbf{m} | \mathcal{X} \setminus \mathbf{m}=\mathbf{x}_o, \mathcal{X} \cap \mathbf{m}=\mathbf{x}_m) = \mathbb{P}(\mathcal{M}=\mathbf{m} | \mathcal{X} \setminus \mathbf{m}=\mathbf{x}_o)$$

X_1	X_2	Y	Weight	Probability ($\epsilon = 10^{-4}$)
0	0	0	$1 - \epsilon$	16.665%
0	1	0	1	16.667%
1	0	0	$1 - \epsilon$	16.665%
1	1	0	1	16.667%
0	0	1	0	0.000%
0	1	1	$1 + \epsilon$	16.668%
1	0	1	0	0.000%
1	1	1	$1 + \epsilon$	16.668%

Table 2: Data distribution over the space $\mathcal{X} \times \mathcal{Y} = \{0, 1\}^2 \times \{0, 1\}$ that serves as the example for the sub-optimality of classification through data-imputation (proof of claim 3).

We have shown that $\mathbb{P}(\mathcal{M}=\mathbf{m} | o(\mathbf{x}, \mathbf{m}), \mathcal{Y} = y)$ does not depend on y , and thus does not affect the optimal prediction rule in claim 1. It may therefore be dropped, and we obtain the marginalized Bayes predictor. \square

Having proved that in the MAR setting, classification through marginalization leads to optimal performance, we now move on to show that the same is not true for classification through data-imputation. Though there are many methods to perform data-imputation, i.e. to complete missing values given the observed ones, all of these methods can be seen as the solution of the following optimization problem, or more typically its approximation:

$$g(\mathbf{x} \odot \mathbf{m}) = \underset{\mathbf{x}' \in \mathbb{R}^s \wedge \forall i: m_i=1 \rightarrow x'_i=x_i}{\operatorname{argmax}} \mathbb{P}(\mathcal{X} = \mathbf{x}')$$

Where $g(\mathbf{x} \odot \mathbf{m})$ is the most likely completion of $\mathbf{x} \odot \mathbf{m}$. When data-imputation is carried out for classification purposes, one is often interested in data-imputation conditioned on a given class $Y = y$, i.e.:

$$g(\mathbf{x} \odot \mathbf{m}; y) = \underset{\mathbf{x}' \in \mathbb{R}^s \wedge \forall i: m_i=1 \rightarrow x'_i=x_i}{\operatorname{argmax}} \mathbb{P}(\mathcal{X} = \mathbf{x}' | \mathcal{Y} = y)$$

Given a classifier $h : \mathbb{R}^s \rightarrow [K]$ and an instance \mathbf{x} with missing values according to \mathbf{m} , classification through data-imputation is simply the result of applying h on the output of g . When h is the optimal classifier for complete data, i.e. the Bayes predictor, we end up with one of the following prediction rules:

$$\text{Unconditional: } h(\mathbf{x} \odot \mathbf{m}) = \underset{y}{\operatorname{argmax}} \mathbb{P}(\mathcal{Y} = y | \mathcal{X} = g(\mathbf{x} \odot \mathbf{m}))$$

$$\text{Conditional: } h(\mathbf{x} \odot \mathbf{m}) = \underset{y}{\operatorname{argmax}} \mathbb{P}(\mathcal{Y} = y | \mathcal{X} = g(\mathbf{x} \odot \mathbf{m}; y))$$

Claim 3. *There exists a data distribution \mathcal{D} and MAR missingness distribution \mathcal{Q} s.t. the accuracy of classification through data-imputation is almost half the accuracy of the optimal marginalized Bayes predictor, with an absolute gap of more than 33 percentage points.*

Proof. For simplicity, we will give an example for a discrete distribution over the binary set $\mathcal{X} \times \mathcal{Y} = \{0, 1\}^2 \times \{0, 1\}$. Let $1 > \epsilon > 0$ be some small positive number, and we define \mathcal{D} according to table 2, where each triplet $(x_1, x_2, y) \in \mathcal{X} \times \mathcal{Y}$ is assigned a positive weight, which through normalization defines a distribution over $\mathcal{X} \times \mathcal{Y}$. The missingness distribution \mathcal{Q} is defined s.t. $P_{\mathcal{Q}}(M_1 = 1, M_2 = 0 | X = \mathbf{x}) = 1$ for all $\mathbf{x} \in \mathcal{X}$, i.e. X_1 is always observed and X_2 is always missing, which is a trivial MAR distribution. Given the above data distribution \mathcal{D} , we can easily calculate the exact accuracy of the optimal data-imputation classifier and the marginalized Bayes predictor under the missingness distribution \mathcal{Q} , as well as the standard Bayes predictor under full-observability. First notice that whether we apply conditional or unconditional data-imputation, and whether X_1 is equal to 0 or 1, the completion will always be $X_2 = 1$ and the predicted class will always be $Y = 1$. Since the data-imputation classifiers always predict the same class $Y = 1$ regardless of their input, the probability of success is simply the probability $P(Y = 1) = \frac{1+\epsilon}{3}$ (for $\epsilon = 10^{-4}$ it equals approximately 33.337%). Similarly, the marginalized Bayes predictor always predicts $Y = 0$ regardless of its input, and so its probability of success is $P(Y = 0) = \frac{2-\epsilon}{3}$ (for $\epsilon = 10^{-4}$ it equals approximately 66.663%), which is almost double the accuracy achieved by the data-imputation classifier. Additionally, notice that the marginalized Bayes predictor achieves almost the same accuracy as the Bayes predictor under full-observability, which equals exactly $\frac{2}{3}$. \square

F Efficient Marginalization with Tensorial Mixture Models

As discussed above, with generative models optimal classification under missing data (in the MAR setting) is oblivious to the specific missingness distribution. However, it requires tractable marginalization over missing values. In this section we show that TMMs bring forth extremely efficient marginalization, requiring only a single forward pass through the corresponding ConvAC.

Recall from sec. 2 and 2.3 that a TMM classifier realizes the following form:

$$P(\mathbf{x}_1, \dots, \mathbf{x}_N | Y=y) = \sum_{d_1, \dots, d_N}^M P(d_1, \dots, d_N | Y=y) \prod_{i=1}^N P(\mathbf{x}_i | d_i; \theta_{d_i}) \quad (9)$$

Suppose now that only the local structures $\mathbf{x}_{i_1} \dots \mathbf{x}_{i_V}$ are observed, and we would like to marginalize over the rest. Integrating eq. 9 gives:

$$P(\mathbf{x}_{i_1}, \dots, \mathbf{x}_{i_V} | Y=y) = \sum_{d_1, \dots, d_N}^M P(d_1, \dots, d_N | Y=y) \prod_{v=1}^V P(\mathbf{x}_{i_v} | d_{i_v}; \theta_{d_{i_v}})$$

from which it is evident that the same network used to compute $P(\mathbf{x}_1, \dots, \mathbf{x}_N | Y=y)$, can be used to compute $P(\mathbf{x}_{i_1}, \dots, \mathbf{x}_{i_V} | Y=y)$ – all it requires is a slight adaptation of the representation layer. Namely, the latter would represent observed values through the usual likelihoods, whereas missing (marginalized) values would now be represented via constant ones:

$$\text{rep}(i, d) = \begin{cases} 1 & , \mathbf{x}_i \text{ is missing (marginalized)} \\ P(\mathbf{x}_i | d; \Theta) & , \mathbf{x}_i \text{ is visible (not marginalized)} \end{cases}$$

More generally, to marginalize over individual coordinates of the local structure \mathbf{x}_i , it is sufficient to replace $\text{rep}(i, d)$ by its respective marginalized mixing component.

To conclude, with TMMs marginalizing over missing values is just as efficient as plain inference – requires only a single pass through the corresponding network. Accordingly, the marginalized Bayes predictor (eq. 3) is realized efficiently, and classification under missing data (in the MAR setting) is optimal (under generative assumption), regardless of the missingness distribution.

G Extended Discussion on Generative Models Based on Neural Networks

There are many generative models realized through neural networks, and convolutional networks in particular. Of these models, one of the most successful to date is the method of Generative Adversarial Networks [19], where a network is trained to generate instances from the data distribution, through a two-player mini-max game. While there are numerous applications for learning to generate data points, e.g. inpainting and super-resolution, it cannot be used for computing the likelihood of the data. Other generative networks do offer inference, but only approximate. Variational Auto-Encoders [24] use a variational lower-bound on the likelihood function. GSNs [5], DPMs [37] and MPDBMs [18] are additional methods along this line. The latter is especially noteworthy for being a generative classifier that can approximate the marginal likelihoods conditioned on each class, and for being tested on classification under missing data.

Some generative neural networks are capable of tractable inference, but not of tractable marginalization. Dinh et al. [15] suggest a method for designing neural networks that realize an invertible transformation from a simple distribution to the data distribution. Inverting the network brings forth tractable inference, yet partial integration of its density function is still intractable. Another popular method for tractable inference, central to both PixelRNN [39] and NADE [38], is the factorization of the probability distribution according to $\mathbb{P}(x_1, \dots, x_d) = \prod_{i=1}^d \mathbb{P}(x_i | x_{i-1}, \dots, x_1)$, and realization of $\mathbb{P}(x_i | x_{i-1}, \dots, x_1)$ as a neural network. Based on this construction, certain marginal distributions are indeed tractable to compute, but most are not. Orderless-NADE partially addresses this issue by using ensembles of models over different orderings of its input. However, it can only estimate the marginal distributions, and has no classifier analogue that can compute class-conditional marginal likelihoods, as required for classification under missing data.

H Image Generation and Network Visualization

Following the graphical model perspective of our models allows us to not only generate random instances from the distribution, but to also generate the most likely patches for each neuron in the network, effectively explaining its role in the classification process. We remind the reader that every neuron in the network corresponds to a possible assignment of a latent variable in the graphical model. By looking for the most likely assignments for each of its child nodes in the graphical tree model, we can generate a patch that describes that neuron. Unlike similar suggested methods to visualize neural networks [40], often relying on brute-force search or on solving some optimization problem to find the most likely image, our method emerges naturally from the probabilistic interpretation of our model.



Figure 5: Generated digits samples from the HT-TMM model trained on the MNIST dataset.

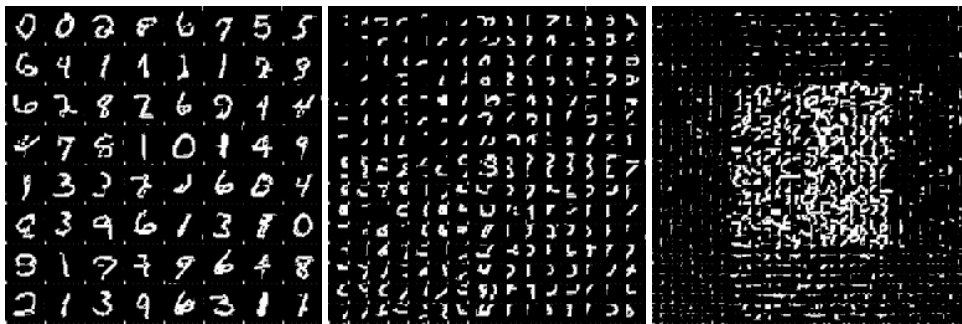


Figure 6: Visualization of the HT-TMM model. Each of the images above visualize a different layer of the model and consists of several samples generated from latent variables at different spatial locations conditioned on randomly selected channels. The leftmost image shows samples taken from the 5th layer which consists of just a single latent variable with 512 channels. The center image shows samples taken from the 4th layer, which consists of 2×2 grid of latent variables with 256 channels each. The image is divided to 4 quadrants, each contains samples taken from the respective latent variable at that position. The rightmost image shows samples from the 3rd layer, which consists of 4×4 grid of latent variables with 128 channels, and the image is similarly spatial divided into different areas matching the latent variables of the layer.

In fig. 5, we can see conditional samples generated for each digit, while in fig. 6 we can see a visualization of the top-level layers of network, where each small patch matches a different neuron in the network. The common wisdom of how ConvNets work is by assuming that simple low-level features are composed together to create more and more complex features, where each subsequent layer denotes features of higher abstraction – the visualization of our network clearly demonstrate this hypothesis to be true for our case, showing small strokes iteratively being composed into complete digits.

I Detailed Description of the Experiments

Experiments are meaningful only if they could be reproduced by other proficient individuals. Providing sufficient details to enable others to replicate our results is the goal of this section. We hope to accomplish this by making our code public, as well as documenting our experiments to a sufficient degree allowing for their reproduction from scratch. Our complete implementation of the models presented in this paper, as well as our modifications to other open-source projects and scripts used in the process of conducting our experiments, are available at our Github repository: <https://github.com/HUJI-Deep/Generative-ConvACs>. We additionally wish to invite readers to contact the authors, if they deem the following details insufficient in their process to reproduce our results.

I.1 Description of Methods

In the following we give concise descriptions of each classification method we have used in our experiments. The results of the experiment on MP-DBM [18] were taken directly from the paper and were not conducted by us, hence we do not cover it in this section. We direct the reader to that article for exact details on how to reproduce their results.

I.1.1 Robust Linear Classifier

In [13], binary linear classifiers were trained by formulating their optimization as a quadric program under the constraint that some of its features could be deleted, i.e. their original value was changed to zero. While the original source code was never published, the authors have kindly agreed to share with us their code, which we used to reproduce their results, but on larger datasets. The algorithm has only a couple hyper-parameters, which were chosen by a grid-search through a cross-validation process. For details on the exact protocol for testing binary classifiers on missing data, please see sec. I.2.1.

I.1.2 K-Nearest Neighbors

K-Nearest Neighbors (KNN) is a classical machine learning algorithm used for both regression and classification tasks. Its underlying mechanism is finding the k nearest examples (called neighbors) from the training set, $(\mathbf{x}_1, y_1), \dots, (\mathbf{x}_k, y_k) \in S$, according to some metric function $d(\cdot, \cdot) : \mathcal{X} \times \mathcal{X} \rightarrow \mathbb{R}_+$, after which a summarizing function f is applied to the targets of the k nearest neighbors to produce the output $y^* = f(y_1, \dots, y_k)$. When KNN is used for classification, f is typically the majority voting function, returning the class found in most of the k nearest neighbors.

In our experiments we use KNN for classification under missing data, where the training set consists of complete examples with no missing data, but at classification time the inputs have missing values. Given an input with missing values $\mathbf{x} \odot \mathbf{m}$ and an example \mathbf{x}' from the training set, we use a modified Euclidean distance metric, where we compare the distance only against the non-missing coordinates of \mathbf{x} , i.e. the metric is defined by $d(\mathbf{x}', \mathbf{x} \odot \mathbf{m}) = \sum_{i:m_i=1} (x'_i - x_i)^2$. Through a process of cross-validation we have chosen $k = 5$ for all of our experiments. Our implementation of KNN is based on the popular *scikit-learn* python library [32].

I.1.3 Convolutional Neural Networks

The most widespread and successful discriminative method nowadays are Convolutional Neural Networks (ConvNets). Standard ConvNets are represented by a computational graph consisted of different kinds of nodes, called layers, with a convolutional-like operators applied to their inputs, followed by a non-linear point-wise activation function, e.g. $\max(0, x)$ known as ReLU.

For our experiments on MNIST, both with and without missing data, we have used the LeNet ConvNet architecture [25] that is bundled with Caffe [23], trained for 20,000 iterations using SGD with 0.9 momentum and 0.01 base learning rate, which remained constant for 10,000 iterations, followed by a linear decrease to 0.001 for another 5,000 iterations, followed by a linear decrease to 0 learning rate for the remaining 5,000 iterations. The model also used l_2 -regularization (also known as weight decay), which was chosen through cross-validation for each experiment separately. No other modifications were made to the model or its training procedure.

For our experiments on NORB, we have used an ensemble of 3 ConvNets, each using the following architecture: 5×5 convolution with 128 output channels, 3×3 max pooling with stride 2, ReLU activation, 5×5 convolution with 128 output channels, ReLU activation, dropout layer with probability 0.5, 3×3 average pooling with stride 2, 5×5 convolution with 256 output channels, ReLU activation, dropout layer with probability 0.5, 3×3 average pooling with stride 2, fully-connected layer with 768 output channels, ReLU activation, dropout layer with probability 0.5, and ends with fully-connected layer with 5 output channels. The stereo images were represented as a two-channel input image when fed to the network. During training we have used data augmentation consisting of randomly scaling and rotation transforms. The networks were trained for 40,000 iterations using SGD with 0.99 momentum and 0.001 base learning rate, which remained constant for 30,000 iterations, followed by a linear decrease to 0.0001 for 6000 iterations, followed by a linear decrease to 0 learning rate for the remaining 4,000 iterations. The model also used 0.0001 weight decay for additional regularization.

When ConvNets were trained on images containing missing values, we passed the network the original image with missing values zeroed out, and an additional binary image as a separate channel, containing 1 for missing values at the same spatial position, and 0 otherwise – this missing data format is sometimes known as *flag data imputation*. Other formats for representing missing values were tested (e.g. just using zeros for missing values), however, the above scheme performed significantly better than other formats. In our experiments, we assumed that the training set was complete and missing values were only present in the test set. In order to design ConvNets that are robust against specific missingness distributions, we have simulated missing values during training, sampling a different mask of missing values for each image in each mini-batch. As covered in sec. 5, the results of training ConvNets directly on simulated missingness distributions resulted in classifiers which were biased towards the specific distribution used in training, and performed worse on other distributions compared to ConvNets trained on the same distribution.

In addition to training ConvNets directly on missing data, we have also used them as the classifier for testing different data imputation methods, as describe in the next section.

I.1.4 Classification Through Data Imputation

The most common method for handling missing data, while leveraging available discriminative classifiers, is through the application of *data imputation* – an algorithm for the completion of missing values – and then passing the results to a classifier trained on uncorrupted dataset. We have tested five different types of data imputation algorithms:

- Zero data imputation: replacing every missing value by zero.
- Mean data imputation: replacing every missing value by the mean value computed over the dataset.
- Generative data imputation: training a generative model and using it to complete the missing values by finding the most likely instance that coincides with the observed values, i.e. solving the following

$$g(\mathbf{x} \odot \mathbf{m}) = \underset{\mathbf{x}' \in \mathbb{R}^s \wedge \forall i, m_i = 1 \rightarrow x'_i = x_i}{\operatorname{argmax}} P(X = \mathbf{x}')$$

We have tested the following generative models:

- Generative Stochastic Networks (GSN) [5]: We have used their original source code from <https://github.com/yaoli/GSN>, and trained their example model on MNIST for 1000 epochs. Whereas in the original article they have tested completing only the left or right side of a given image, we have modified their code to support general masks. Our modified implementation can be found at <https://github.com/HUJI-Deep/GSN>.
- Non-linear Independent Components Estimation (NICE) [15]: We have used their original source code from <https://github.com/laurent-dinh/nice>, and trained it on MNIST using their example code without changes. Similarly to our modification to the GSN code, here too we have adapted their code to support general masks over the input. Additionally, their original inpainting code required 110,000 iterations, which we have reduced to just 8,000 iterations, since the effect on classification accuracy was marginal. For the NORB dataset, we have used their CIFAR10 example, with lower learning rate of 10^{-4} . Our modified code can be found at <https://github.com/HUJI-Deep/nice>.
- Diffusion Probabilistic Models (DPM) [37]: We have user their original source code from <https://github.com/Sohl-Dickstein/Diffusion-Probabilistic-Models>, and trained it on MNIST using their example code without changes. Similarly to our modifications to GSN, we have add support for a general mask of missing values, but other than that kept the rest of the parameters for inpainting unchanged. For NORB we have used the same model as MNIST. We have tried using their CIFAR10 example for NORB, however, it produced exceptions during training. Our modified code can be found at <https://github.com/HUJI-Deep/Diffusion-Probabilistic-Models>.

I.1.5 Tensorial Mixture Models

For a complete theoretical description of our model please see the body of the article. Our models were implemented by performing all intermediate computations in log-space, using numerically aware operations. In practice, that meant our models were realized by the SimNets architecture [7, 10], which consists of Similarity layers representing gaussian distributions, MEX layers representing weighted sums performed on log-space input and outputs, as well as standard pooling operations. The learned parameters of the MEX layers are called *offsets*, which represents the weights of the weighted sum, but saved in log-space. The parameters of the MEX layers can be optionally shared between spatial regions, or alternatively left with no parameter sharing at all. Additionally, when used to implement our generative models, the offsets are normalized to have a soft-max (i.e., $\log(\sum_i \exp(x_i))$) of zero.

The network architectures we have tested in this article, consists of M different Gaussian mixture components with diagonal covariance matrices, over non-overlapping patches of the input of size 2×2 , which were implemented by a similarity layer as specified by the SimNets architecture, but with an added gaussian normalization term.

We first describe the architectures used for the MNIST dataset. For the CP-TMM model, we used $M = 800$, and following the similarity layer is a 1×1 MEX layer with no parameter sharing over spatial regions and 10 output channels. The model ends with a global sum pooling operation, followed by another 1×1 MEX layer with 10 outputs, one for each class. The HT-TMM model starts with the similarity layer with $M = 32$, followed by a sequence of four pairs of 1×1 MEX layer followed by 2×2 sum pooling layer, and after the pairs and additional 1×1 MEX layer lowering the outputs of the model to 10 outputs as the number of classes. The number of output channels for each MEX layer are as follows 64-128-256-512-10. All the MEX layers in this network do not use parameter sharing, except the first MEX layer, which uses a repeated sharing pattern of 2×2 offsets, that analogous to a 2×2 convolution layer with stride 2. Both models were trained with the losses described in sec. 2.3, using the Adam SGD variant for optimizing the parameters, with a base learning rate of 0.03, and $\beta_1 = \beta_2 = 0.9$. The models were trained for 25,000 iterations, where the learning rate was dropped by 0.1 after 20,000 iterations.

For the NORB dataset, we have trained only the HT-TMM model with $M = 128$ for the similarity layer. The MEX layers use the same parameter sharing scheme as the one for MNIST, and the number of output channels for each MEX layer are as follows: 256-256-256-512-5. Training was identical to the MNIST models, with the exception of using 40,000 iterations instead of just 25,000. Additionally, we have used an ensemble of 4 models trained separately, each trained using a different generative loss weight (see below for more information). We have also used the same data augmentation methods (scaling and rotation) which were used in training the ConvNets for NORB used in this article.

The standard L_2 weight regularization (sometimes known as weight decay) did not work well on our models, which lead us to adapt it to better fit to log-space weights, by minimizing $\lambda \sum_i (\exp(x_i))^2$ instead of $\lambda \|\mathbf{x}\|_2^2 = \lambda \sum_i \mathbf{x}_i^2$, where the parameter λ was chosen through cross-validation. Additionally, since even with large values of λ our model was still overfitting, we have added another form of regularization in the form of *random marginalization* layers. A random marginalization layer, is similar in concept to dropout, but instead of zeroing activations completely in random, it choses spatial locations at random, and then zero out the activations at those locations for all the channels. Under our model, zeroing all the activations in a layer at a specific location, is equivalent to marginalizing over all the inputs for the receptive field for that respective location. We have used random marginalization layers in between all our layers during training, where the probability for zeroing out activations was chosen through cross-validation for each layer separately. Though it might raise concern that random marginalization layers could lead to biased results toward the missingness distributions we have tested it on, in practice the addition of those layers only helped improve our results under cases where only few pixels where missing.

Finally, we wish to discuss a few optimization tricks which had a minor effects compared to the above, but were nevertheless very useful in achieving slightly better results. First, instead of optimizing directly the objective defined by eq. 2, we add smoothing parameter β between the two terms, as follows:

$$\Theta^* = \underset{\Theta}{\operatorname{argmin}} - \sum_{i=1}^{|S|} \log \frac{e^{N_{\Theta}(X^{(i)}, Y^{(i)})}}{\sum_{y=1}^K e^{N_{\Theta}(X^{(i)}, y)}} - \beta \sum_{i=1}^{|S|} \log \sum_{y=1}^K e^{N_{\Theta}(X^{(i)}, y)}$$

setting β too low diminish the generative capabilities of our models, while setting it too high diminish the discriminative performance. Through cross-validation, we decided on the value $\beta = 0.01$ for the models trained on MNIST, while for NORB we have used a different value of β for each of the models, ranging in $\{0.01, 0.1, 0.5, 1\}$. Second, we found that performance increased if we normalized activations before applying the 1×1 MEX operations. Specifically, we calculate the soft-max over the channels for each spatial location

which we call the activation norm, and then subtract it from every respective activation. After applying the MEX operation, we add back the activation norm. Though might not be obvious at first, subtracting a constant from the input of a MEX operation and adding it to its output is equivalent does not change the mathematical operation. However, it does resolve the numerical issue of adding very large activations to very small offsets, which might result in a loss of precision. Finally, we are applying our model in different translations of the input and then average the class predictions. Since our model can marginalize over inputs, we do not need to crop the original image, and instead mask the unknown parts after translation as missing. Applying a similar trick to standard ConvNets on MNIST does not seem to improve their results. We believe this method is especially fit to our model, is because it does not have a natural treatment of overlapping patches like ConvNets do, and because it is able to marginalize over missing pixels easily, not limiting it just to crop translation as is typically done.

I.2 Description of Experiments

In this section we will give a detailed description of the protocol we have used during our experiments.

I.2.1 Binary Digit Classification under Feature Deletion Missing Data

This experiment focuses on the binary classification problem derived from MNIST, by limiting the number of classes to two different digits at a time. We use the same non-zero feature deletion distribution as suggested by Globerson and Roweis [17], i.e. for a given image we uniformly sample a set of N non-zero pixels from the image (if the image has less than N non-zero pixels then they are non-zero pixels are chosen), and replace their values with zeros. This type of missingness distribution falls under the MNAR type defined in sec.3.

We test values of N in $\{0, 25, 50, 75, 100, 125, 150\}$. For a given value of N , we train a separate classifier on each digit pair classifier on a randomly picked subset of the dataset containing 300 images per digit (600 total). During training we use a fixed validation set with 1000 images per digit. After picking the best classifier according to the validation set, the classifier is tested against a test set with a 1000 images per digits with a randomly chosen missing values according to the value of N . This experiment is repeated 10 times for each digit pair, each time using a different subset for the training set, and a new corrupted test set. After conducting all the different experiments, all the accuracies are averaged for each value of N , which are reported in table 1.

I.2.2 Multi-class Digit Classification under MAR Missing Data

This experiment focuses on the complete multi-class digit classification of the MNIST dataset, in the presence of missing data according to different missingness distributions. Under this setting, only the test set contains missing values, whereas the training set does not. We test two kinds of missingness distributions, which both fall under the MAR type defined in sec.3. The first kind, which we call *i.i.d. corruption*, each pixel is missing with a fixed probability p . the second kind, which we call *missing rectangles corruption*, The positions of N rectangles of width W or chosen uniformly in the picture, where the rectangles can overlap one another. During the training stage, the models to be tested are not to be biased toward the specific missingness distributions we have chosen, and during the test stage, the same classifier is tested against all types of missingness distributions, and without supplying it with the parameters or type of the missingness distribution it is tested against. This rule prevent the use of ConvNets trained on simulated missingness distributions. To demonstrate that the latter lead to biased classifiers, we have conducted a separate experiment just for ConvNets, where the previous rule is ignored, and we train a separate ConvNet classifier on each type and parameter of the missingness distributions we have used. We then tested each of those ConvNets on all other missingness distributions, the results of which are in fig. 3, which confirmed our hypothesis.